REPORT DOCUMENTATION PAGE

Form Approved
OMB No. 0704-0188

1. AGENCY USE ONLY *(Leave blank)*

2. REPORT DATE
February 1999

3. REPORT TYPE AND DATES COVERED
Annual (15 Sep 97 - 14 Sep 98)

4. TITLE AND SUBTITLE
X-ray Crystallographic Studies on Acetylcholinesterase and Related Enzymes

5. FUNDING NUMBERS
DAMD17-97-2-7022

6. AUTHOR(S)
J. L. Sussman, Ph.D. and I. Silman, Ph.D.

7. PERFORMING ORGANIZATION NAME(S) AND ADDRESS(ES)
Weizmann Institute of Science
Rehovot 76100, Israel

8. PERFORMING ORGANIZATION REPORT NUMBER

9. SPONSORING / MONITORING AGENCY NAME(S) AND ADDRESS(ES)
U.S. Army Medical Research and Materiel Command
Fort Detrick, MD 21702-5012

10. SPONSORING / MONITORING AGENCY REPORT NUMBER

11. SUPPLEMENTARY NOTES

12a. DISTRIBUTION / AVAILABILITY STATEMENT
Approved for public release; distribution unlimited

12b. DISTRIBUTION CODE

13. ABSTRACT *(Maximum 200 words)*

19990709003

14. SUBJECT TERMS
Chemical Defense

15. NUMBER OF PAGES
55

16. PRICE CODE

17. SECURITY CLASSIFICATION OF REPORT	18. SECURITY CLASSIFICATION OF THIS PAGE	19. SECURITY CLASSIFICATION OF ABSTRACT	20. LIMITATION OF ABSTRACT
Unclassified	Unclassified	Unclassified	Unlimited

AD ______

COOPERATIVE AGREEMENT NO:DAMD17-97-2-7022

TITLE X-RAY CRYSTALLOGRAPHIC STUDIES ON ACETYLCHOLINESTERASE AND RELATED ENZYMES

PRINCIPAL INVESTIGATORS: J. L. SUSSMAN, Ph.D.
I. SILMAN, Ph.D.

CONTRACTING ORGANIZATION: Weizmann Institute of Science
Departments of Structural Biology & Neurobiology
Rehovot 76100, Israel

REPORT DATE: February 1999

TYPE OF REPORT: Annual Report

PREPARED FOR: U.S. Army Medical Research and Materiel Command
Fort Detrick, Frederick, MD 21702-5012

DISTRIBUTION STATEMENT: Approved for public release;
distribution unlimited.

FOREWORD

Options, interpretations, conclusions and recommendations are those of the author and are not necessarily endorsed by the U.S. Army.

_____ Where copyrighted material is quoted, permission has been obtained to use such material.

_____ Where material from documents designed for limited distribution is quoted, permission has been obtained to use the material.

_____ Citations of commercial organizations and trade names in this report do not constitute an official Department of the Army endorsement or approval of the products or services of these organizations.

_____ In conducting research using animals, the investigator(s) adhered to the "Guide for the Care and Use of Laboratory Animals," prepared by the Committee on Care and Use of Laboratory Animals of the Institute of Laboratory Resources, National Research Council (NIH Publication No. 86-23, Revised 1985).

_____ For the protection of human subjects, the investigator(s) adhered to policies of applicable Federal Law 45 CFR 46.

_____ In conducting research utilizing recombinant DNA technology, the investigator(s) adhered to current guidelines promulgated by the National Institutes of Health.

2/17/99

PI - Signature DATE

SUMMARY

The principal objectives of the current project included:

1. Work on *Torpedo* acetylcholinesterase (*Tc*AChE) involving two principal topics:
   A) Preparation and characterization of 'aged' and 'non-aged' organophosphoryl (OP) conjugates.
   B) Use of time-resolved crystallography in order to understand the mechanism of action of acetylcholinesterase (AChE), as well as the traffic of substrate and products through the active-site gorge.
2. Structural studies on other cholinesterases (ChEs).
3. Homology model building and detailed structural comparison of human, bovine fetal serum, snake venom and insect AChE, and of horse and human serum butyrylcholinesterase (BChE).
4. Structural studies on human paraoxonase.

In the first year of this project, we have made progress towards all four objectives, as well as in additional areas related to the long-term aims of our research program, as follows:

A. The structures of aged conjugates obtained by reaction of *Tc*AChE with di*iso*propylphosphorofluoridate (DFP), *O-iso*propylmethylphosponofluoridate (sarin), and *O*-pinacolylmethylphosphonofluoridate (soman) were solved by X-ray crystallography to 2.3, 2.5 and 2.2Å resolution, respectively.

B. Laue X-ray data were collected at the Third Generation Synchrotron, *i.e.* the European Synchrotron Research Facility (ESRF), Grenoble, on trigonal crystals of *Tc*AChE complexed with edrophonium (EDR). Data were collected in msec and µs time slices; even with such exposure times, it was possible to obtain electron density maps comparable in quality to those obtained from monochromatic data.

C. The 3D structure of a complex of human recombinant AChE with the snake venom toxin, fasciculin, has been determined to 2.7Å resolution. A similar data set has been collected for a complex with fasciculin of the human recombinant E202Q mutant.

D. Homology models have been constructed, on the basis of the *Tc*AChE structure, for human, *Bungarus fasciatus* and *Drosophila melanogaster* AChE's, and for human BChE. Modelling reveals that the overall charge asymmetry, first observed for the *Torpedo* enzyme, is conserved throughout the ChE family.

E. A number of neural cell-adhesion proteins, including gliotactin, neurotactin, and neuroligin, have substantial sequence homology to the ChEs. Homology models of these proteins showed that their electrostatic characteristics were similar to those of the AChEs, with which they share a negative electrostatic motif, which, in AChE, is located around the entrance to the active-site gorge.

F. Cloning and expression studies of human paraoxonase have been initiated.

TABLE OF CONTENTS

OBJECTIVES

The principal objectives of this contract are to better understand the mechanism of action of AChE, and to characterize its various ligand-binding sites. These objectives are being approached by the method of single crystal X-ray diffraction, together with time-resolved X-ray crystallography, using *Torpedo californica* AChE (*Tc*AChE) as the principal source of enzyme. Computational molecular model building and electrostatic characterization are being used as complementary theoretical approaches. Attempts are also being made to crystallize, and if successful, to solve the 3D structures of cholinesterases (ChEs) from other sources. These include human recombinant AChE, bovine fetal serum AChE, AChE from the venom of the krait, *Bungarus fasciatus* (*Bf*AChE), and horse serum BChE. Homology model building will be used to compare and analyze the structures of these enzymes. In parallel, we are attempting to express and crystallize, with the eventual objective of solving its 3D structure, human serum paraoxonase/arylesterase.

1. Work on *Tc*AChE involves two principal topics:

A) Preparation and characterization of 'aged' and 'non-aged' OP conjugates, with the objective of fully understanding the mechanistic basis and specificity of interaction of organophosphates and organophosphonates of therapeutic and toxicological interest with the active site of AChE, as well as the molecular basis of the 'aging' process.

B) Use of time-resolved crystallography in order to understand the mechanism of action of AChE, as well as the traffic of substrate and products through the active-site gorge. The experimental approaches to be adopted will be Laue crystallography and ultra-rapid freezing time-resolved crystallography. In either case, time-resolved data collection will be preceded by synthesis and characterization of suitable caged compounds, and by a study of their interaction with *Tc*AChE, initially in solution and, subsequently, under steady-state X-ray data collection conditions.

2. Work on other ChEs obviously depends on the success of crystallization attempts. Particular attention is being paid to human AChE (hAChE), in view of its toxicological and therapeutic importance. In the first year of the contract, we have devoted substantial efforts to improving purification techniques already developed in our own laboratory for processing culture media containing recombinant hAChE (rhAChE), supplied by the group of Dr. Avigdor Shafferman at the Israel Institute for Biological Research (IIBR).

3. Homology model building and detailed structural comparison of human, bovine fetal serum, snake venom and insect AChE, and of horse and human serum BChE.

4. Work on paraoxonase is subject to the same restrictions as for the various ChEs, namely the availability of crystals. Thus expression and purification will precede data collection and structure determination.

BACKGROUND

Acetylcholinesterase

Acetylcholinesterase (AChE) plays a key role in cholinergic neurotransmission. By rapid hydrolysis of the neurotransmitter, acetylcholine (ACh), it terminates the chemical impulse, thereby permitting rapid repetitive responses (1). AChE is, accordingly, characterized by a remarkably high specificity, especially for a serine hydrolase (2), functioning at a rate approaching that of a diffusion-controlled reaction (3, 4). The powerful acute toxicity of organophosphorus (OP) poisons (as well as of carbamates and sulfonyl halides which function analogously) is attributed primarily to the fact that they are potent inhibitors of AChE (5, 6). Inhibition is achieved by their covalent attachment to a serine residue within the active site (2, 7). AChE inhibitors are utilized in treatment of various disorders such as myasthenia gravis and glaucoma (6, 8). More recently, they have been under active consideration for use in the management of Alzheimer's disease (9, 10). The cholinesterase inhibitors, tacrine, under the trade name Cognex®, and E2020, under the trade name Aricept®, have both been approved for use by the FDA (11, 12). Elucidation of the 3D structure of AChE is, therefore, of fundamental interest for understanding its remarkable catalytic efficacy, and of applied importance in drug design and in developing therapeutic approaches to OP poisoning. Furthermore, information concerning the ACh-binding site of AChE is pertinent to an understanding of the molecular basis for the recognition of ACh by other ACh-binding proteins such as the various ACh receptors (13-15).

Crystallization and determination of the 3D structure of AChE from *Tc*AChE (16, 17) enabled us to visualize, for the first time, at atomic resolution, a binding pocket for ACh. It also allowed us to identify the active site of AChE, which is located at the bottom of a deep gorge lined largely by aromatic residues (17, 18). This unusual and unexpected structure gives us the opportunity to work out structure-function relationships of AChE. Furthermore, the so-called 'anionic' binding site for the quaternary moiety of ACh does not contain several negative charges, as was earlier postulated on the basis of the ionic-strength dependence of catalytic activity (19). Our modeling studies (17) suggested that the quaternary group interacts primarily with the indole ring of the conserved tryptophan residue, W84; this was borne out by crystallographic studies on several AChE-ligand complexes, complemented by photoaffinity labeling, which also suggested a prominent role for another conserved aromatic residue, F330 (20, 21).

The availability of the 3D structure of *Tc*AChE stimulated a large body of work, in several laboratories, which shared the common objective of correlating the unexpected structure revealed by X-ray crystallography with the catalytic function of the enzyme. These studies can be loosely classed in four main categories, two theoretical and two experimental (some studies encompass more than one category):

1) Theoretical studies, in which the structure of AChE or BChE from various sources is modeled on the basis of the 3-D structure of *Tc*AChE, together with the amino acid sequence of the ChE in question, obtained from cloning and/or sequencing studies. Such modeling is

possible due to the high sequence homology that exists between ChEs of differing phylogenetic origin (22, 23).

2) Theoretical studies aimed at elucidating the electrostatic and dynamic properties of the ChE molecule and their contribution to known catalytic properties.

3) Experimental investigations concerned with understanding the catalytic and ligand-binding properties of the ChEs on the basis of kinetic and spectroscopic studies with AChE and BChE from various sources.

4) Studies using site-directed mutagenesis to understand the contribution of particular amino acid residues to catalytic activity, substrate specificity, and mode of interaction with reversible and covalent inhibitors.

Inspection of the 3D structures of *Tc*AChE and of various AChE-ligand complexes, as well as of the structure of homologous enzymes, led to predictions concerning the involvement of certain amino acid residues, almost all localized in the 'aromatic gorge', in various aspects of catalytic activity. Site-directed mutagenesis was the principle tool for testing such predictions. Thus, on the basis of the topology of the gorge (17), of the X-ray structure of complexes of *Tc*AChE with the bisquaternary inhibitors decamethonium (20) and BW284c51 (Harel *et al.*, unpublished), and on the modeling of hBChE (23), it was suggested that the so-called 'peripheral' anionic site, previously identified from kinetic (24) and spectroscopic studies (25, 26), is located at the top of the gorge. Like the 'anionic' subsite of the active site, it was thought to contain three aromatic residues, Y70, Y121, and W279 (*Torpedo* numbering is used here and subsequently). Kinetic comparisons with hBChE, which lacks these three residues, and with chicken AChE, which lacks two of them, provided strong experimental evidence to support this prediction (23, 27-30). In addition, a role for the acidic residue, D72, in the 'peripheral' site, was proposed on the basis of site-directed mutagenesis (31). Modeling also suggested that two aromatic residues, F288 and F290, confer narrow substrate specificity upon AChE compared to BChE (32, 33); this suggestion, too, was clearly borne out by mutagenesis studies. Thus, our computer modeling had high predictive capacity, and we are now modeling hAChE similarly, as well as more distantly related enzymes, *e.g.* insect AChEs, in the context of insecticide development.

Studies carried out to date have involved about 200 mutations, principally of hAChE, mouse AChE (mAChE), *Tc*AChE, *Torpedo marmorata* AChE (*Tm*AChE) and *Drosophila melanogaster* AChE (*Dm*AChE), as well as of hBChE (34). An updated compilation of these mutations can be obtained by accessing the Cholinesterase Data Base, at Montpellier, France, maintained by A. Chatonnet (see: http://www.ensam.inra.fr/cholinesterase/). These mutagenesis studies leave open numerous questions. Thus, the present data ascribe firm roles to about half of the conserved aromatic residues in the gorge, and the role of the remainder is either not fully established or unknown. Furthermore, the role of two acidic residues, E199 and D72, the former near the bottom of the gorge and the latter close to the top, is not clearly ascertained, and the long-standing question of the molecular basis for substrate inhibition is still unresolved. The attractive possibility that substrate inhibition involves binding of a second ACh molecule at the 'peripheral' site (27) is prejudiced by a number of studies. These involve mutagenesis of aromatic residues at the 'peripheral' site (28, 35) and comparative studies on the chicken and *Torpedo* enzymes (30), as well as the observation that mutation of E199 strongly reduces substrate inhibition (36). A complication in analyzing all the site-directed mutagenesis data is that, in certain cases, mutations at the top of the gorge appear to affect parameters ascribed to structural factors associated with the bottom of the gorge, and *vice versa* (31). This is of interest, because it provides evidence that the gorge may function in an integrated fashion, but also means that interpretation of individual site-directed mutagenesis experiments must be treated with caution.

Paraoxonase

Paraoxonase (EC 3.1.8.1) belongs to the family of A-esterases as defined by Aldridge (37), which are capable of hydrolyzing OPs, carbamates and aromatic carboxylic acid esters. They have been the subject of a substantial research effort due to their potential capacity to offer protection against intoxication by paraoxon and by other OPs, which might serve as insecticides. Indeed, there is evidence to support the notion that serum paraoxonase plays a significant role in the detoxification of paraoxon in the rabbit *in vivo* (38). Paraoxonase may also confer protection on coronary artery disease by destroying pro-inflammatory oxidized lipids present in oxidized low-density lipoproteins (LDLs). Indeed, paraoxonase knock-out mice are susceptible both to OP toxicity and to atherosclerosis (39).

OP-hydrolyzing activity has been described throughout the phylogenetic tree from microorganisms up to several mammalian species (40, 41). It remains to be established whether various esterases capable of hydrolyzing OP in different organisms *e.g.* the diisopropylphosphofluoridate hydrolase (DFPase) of the squid head ganglion (42), are homologous members of a small number of families displaying substantial structural similarity. In the case of a phosphotriesterase from *Pseudomonas*, which is known to hydrolyze both paraoxon and parathion (43), it has been clearly established that it shows no homology with the human enzyme, which does not hydrolyze parathion (44). The molecular structure of the phosphotriesterase has recently been solved to 2.1Å resolution (45, 46). From the 3D structure, together with kinetic and chemical data on this enzyme (47, 48), it does not appear to be closely related to human paraoxonase.

The human serum enzyme which hydrolyses paraoxon is known as human paraoxonase/arylesterase (PON1), due to its high activity on aryl esters (49). It has been investigated extensively by the laboratories of Furlong (50) and La Du (44). Thus it has been purified to homogeneity (51), and also cloned and expressed (52, 53). It occurs in two isozymic forms, A and B, whose pharmacogenetics have been worked out by the two laboratories. The two forms differ substantially in their specific activity towards various substrates. Notably, the B-type hydrolyses paraoxon over 6-fold faster than the A-type at high ionic strength, and hydrolyses 2-naphthyl acetate 2.5-fold faster.

The laboratory of La Du has developed a procedure for purification of PON1 from human serum (51) which allowed them to obtain both the A- and B-type enzymes purified over 500-fold (54). PON1 binds tightly to apolipoproteins, and also displays a tendency to aggregate, properties which necessitate purification in the presence of a non-ionic detergent and glycerol. The purified enzyme is stable for months when stored at 4°C in the presence of glycerol, a non-ionic detergent, and Ca^{++}; the divalent cation is essential for maintenance of the native conformation. By this procedure, PON1 was prepared in 10 mg batches, which permitted preliminary screening of crystallization conditions. Indeed, we were able to obtain some microcrystals from one such batch.

The polypeptide chain of PON1 contains 354 amino acids, and ca. 16% carbohydrate, which is attached at three glycosylation sites. La Du and coworkers (52) detected two amino acid residues, 54 and 191, which might provide the structural basis for the A/B polymorphism. Subsequent molecular genetic and nucleotide sequencing studies by the La Du and Furlong groups (53, 55) showed that the Arg/Gln polymorphism, which is observed at residue 191, follows exactly the A/B phenotype of human PON1. No influence on the enzyme has yet been observed of the Met/Leu polymorphism which is commonly observed at residue 54.

RESULTS

Acetylcholinesterase from TcAChE

a) The structure of 'aged' OP conjugates of *Tc*AChE

OP inhibitors react rapidly with AChE, and may then undergo post-inhibitory reactions to produce an irreversibly inhibited, 'aged' OP-enzyme conjugate. To understand the structural basis for the non-reactivatibility of aged OP-AChE conjugates, we crystallized and solved the X-ray structures of conjugates obtained by reaction of *Tc*AChE with DFP, sarin or soman. The stoichiometric conjugates were produced in collaboration with the group of Dr. Avigdor Shafferman at IIBR. After they had been shown to be fully inactivated (>99%) and aged (>95%), each conjugate was crystallized from PEG200 under conditions similar to those employed for native *Tc*AChE (56).

Two different crystal forms suitable for X-ray diffraction studies appeared in drops containing the aged OP-*Tc*AChE conjugates: orthorhombic space group $P2_12_12_1$ and trigonal space group $P3_121$. X-ray data were collected using trigonal crystals, and finally refined at 2.4Å (DFP), 2.5Å (sarin), and 2.2Å (soman) resolution. The highest positive difference density peak, corresponding to the OP, was observed to be within covalent bonding distance of the Oγ of Ser200 in each structure (Fig. 1). The final reaction product was methylphosphonylated (MeP)-AChE for both soman and sarin (Fig. 2), and mono*iso*propylphosphorylated (MiPrP)-AChE with DFP (Fig. 3).

The large molar excess of sarin or soman used should have resulted in almost exclusive reaction of AChE with the toxic, P(S) stereoisomers (57). Assuming no reorientation of the inhibitor in the active site during aging, the absolute configuration of the OP adduct in the MeP-AChE structures is consistent with a simple in-line nucleophilic attack and inversion of stereochemistry at the phosphorus atom during phosphonylation. The inversion mechanism has been proposed for AChE by analogy with other serine hydrolases (58). Comparison of the aged sarin and DFP conjugates, both of which have lost an *iso*propyl group during aging, supports this conclusion.

The primary problem created by the dealkylation reaction of aging is the introduction of a formal negative charge, because anionic phosphoesters are inherently resistant to nucleophilic attack (59). Specific interactions between the enzyme's active site and the OP almost certainly add to the stability of aged AChE, however, because denaturation of aged M*i*PrP-AChE does permit base-catalyzed dephosphorylation (60).

A hydrogen bond from Nε2 of the active site imidazolium to one oxygen atom of the anionic OP conjugate has been postulated to be a key interaction that stabilizes both aged M*i*PrP-trypsin (61, 62) and M*i*PrP-chymotrypsin (63). Active site distances and angles of the three solved OP-AChE structures are consistent with the formation of such an H-bond.

Our results reinforce the conclusion that there are multiple factors militating against reactivation of aged AChE: (i) the anionic character of the phosphoester; (ii) three potential H-bond donors from the oxyanion hole to one of the oxygen atoms bound to P; (iii) an additional H-bond from the His440 Nε2 to the other oxygen atom; and (iv) the wrong protonation state and poor geometry for His440 to act as a general base catalyst.

The phosphonyl oxygen atoms may carry significantly greater fractional negative charges than do the oxygens of the ACh transition state (TS) adduct (*cf.*, (58) and (62)). Despite this limitation, the active sites of MeP-AChE should provide useful structural analogs for modeling the deacylation TS formed by the natural substrate (ACh) (62, 64, 65).

The position of the phosphonyl oxygen should mimic that of the TS carbonyl oxygen. All three OP structures corroborate that the oxyanion is stabilized in AChE by potential H-bonds from the amide nitrogens of G118, G119 and A201 (Figs. 2, 3). This is consistent with the preliminary model for the binding of ACh to native AChE (17), as well as with the structure of a complex of a transition state analog, namely *m*-(N,N,N-trimethylammonio)trifluoroacetophenone (TMTFA) with *Tc*AChE (21).

A hydrophobic pocket which surrounds the phosphonate methyl group is formed in *Tc*AChE by W233, F288, and F290. F331 may contribute to the acyl pocket by providing π-π-interactions with F288. Both F288 and F290 provide close non-bonded contacts to the sarin or soman methyl group (Fig. 2), suggesting that these aromatic side chains form a specific pocket for the methyl of the acetyl group of ACh. Contacts from the acyl pocket to the phosphonate methyl group are generally closer than those observed for the CF_3 group of TMTFA.

Structure-activity studies with carboxyl ester substrates and OP inhibitors first suggested the presence of specific binding pockets in the active site of AChE that complement the acyl and alkoxy groups (reviewed in (66, 67)). Furthermore, this approach showed convincingly that the acyl pocket of AChE was more restricted than that of the closely related enzyme, BChE. When the crystal structure of AChE became available, homology models of BChE were built and, by inference from site-specific mutagenesis results, two aromatic residues, F288 and F290, were implicated as the source of greater selectivity of AChE (29, 33, 36). The pocket of BChE was viewed as more "open" because it contained Leu and Val (or Ile) residues at these positions, whereas the two Phe residues in the pocket of AChE were described as a "clamp" for the methyl group of ACh that would poorly accommodate bulkier acyl groups (36).

DFP binds >150-fold more tightly to BChE than to AChE (68). Using mutagenesis and a series of OPs, it was shown that the relatively poor binding of DFP could be accounted for almost completely by an increase in the K_d of the hAChE-DFP reversible complex. This increase was mediated primarily by F295 and, to a lesser extent by F297, corresponding to residues F288 and F290, respectively, in *Tc*AChE (69).

We observed the first major conformational change in a *Tc*AChE complex for the M*i*PrP-AChE structure (obtained after reaction with DFP; Fig. 3). Significant movement of the main chain atoms allows repositioning of F288 and F290 to accommodate the remaining *iso*propyl group of the OP in the 'aged' conjugate. Superposing the MiPrP-AChE structure with native *Tc*AChE showed that DFP causes the Cα atoms at positions 288-290 to move more than 3.0Å. The free energy penalty associated with this movement probably explains the reduced binding affinity of AChE, relative to BChE, for DFP, the P(R) phosphonates, and other substrates or inhibitors with bulky acyl groups. The conformational change in the acyl pocket observed by X-ray crystallography belies earlier molecular modeling studies, which generally predicted that the degrees of freedom available to the substrate or inhibitor were restricted by F288 and F290, and not that AChE itself undergoes a major conformational movement of the main chain to accommodate bulky ligands.

Although there is evidence for conformational changes associated with aging of some OP-AChE, -BChE, or -chymotrypsin conjugates in solution (70-72), we found no major structural rearrangements in *Tc*AChE as a result of the aging reaction itself. The root mean square deviation found by comparing the Cα atoms of either MeP-AChE structure with native AChE was less than 0.3Å. Moreover, superposing the active site residues of each MeP-AChE with those of native 2ACE, as well as with thirteen other previously solved *Tc*AChE structures, showed no significant movements that could be attributed to aging. It remains possible, however, that a transient conformational change occurs on the pathway to the final aged structure observed by X-ray crystallography. This possibility may be investigated by solution studies, as well as by ongoing X-ray crystallographic studies of non-aged OP-AChE complexes.

b) X-ray Laue studies on *Tc*AChE

As already mentioned, AChE is an extremely efficient catalyst, with a turn-over number of ~20,000 per second (2). The X-ray structure of *Tc*AChE (17) unexpectedly revealed that the active-site is buried within the protein, apparently accessible only via a long and narrow gorge lined with aromatic residues. Furthermore, the AChE molecule displays an asymmetric charge distribution, resulting in a strong dipole moment, aligned approximately along the active-site gorge (73, 74). It was suggested that the electric field so generated attracts the positively charged ACh to the rim of the gorge (73). The substrate is then guided by the electric field, using the aromatic residues in the gorge as a series of low-affinity sites, towards the active site. The narrow dimensions of the active-site gorge, taken together with the potential gradient along it, raise cogent questions regarding traffic of substrate and products to and from the active site. Thus, in addition to steric considerations, the potential along the gorge would be expected to accelerate expulsion of acetate from the active site, but retard release of choline. Furthermore, movement of water between the bulk phase and the gorge must be taken into account. It was, therefore, suggested that the reaction products, choline in particular, might leave the active site through a "back door", a transient opening in the thin aspect of the gorge wall, produced by movement of one or more amino acid residues (73, 75, 76). Residues that might contribute to the opening of such a putative back door would most likely be located on the Ω loop between C67 and C94 in *Tc*AChE (18), a loop which is known to adopt an open and closed conformation in the structurally similar enzyme, *Candida rugosa* lipase (77). Further evidence for an alternative entrance to the gorge comes from studies on the mode of inhibition of AChE by the potent snake venom polypeptide toxin, fasciculin. Crystallographic studies demonstrate that the toxin completely blocks the entrance to the active-site gorge (78, 79). Nevertheless, significant residual catalytic activity can be observed in solution (80). However, site-directed mutagenesis studies which were designed to prove the importance of the mobility of certain residues, did not provide support for the existence of a back door (76, 81).

Time-resolved crystallography is clearly an approach with the potential to provide direct experimental information to either support or refute the existence of a “back door”. The Laue diffraction method has been employed successfully in recent years to observe enzyme reactions as they occur in the crystal state (82, 83). The technique is attractive due to the very short exposure times required. Recently, crystallographic snapshots of structural changes occurring in a protein on a time scale as short as nanoseconds have been reported (84). A prerequisite for successful Laue measurements is achievement of a high degree of synchronization of the initialisation of the reaction. In some cases, the substrate is immobilized by attachment of a photosensitive chemical moiety, effectively turning it into an inhibitor. Such caged compounds can then be activated by photolysis, usually with laser flashes. In the case of AChE, a series of caged compounds has been synthesized, and characterized photochemically and enzymatically, which generate either choline or carbamylcholine upon photolysis (85, 86). CCh is a substrate of AChE; the first step of the reaction, carbamylation of the enzyme, is rapid, but decarbamylation is slow, on a time scale of minutes at room temperature (87). It is envisaged that synchronized photolysis of caged CCh within the crystal will produce rapid release of choline by the enzymatic machinery, and that movement of choline, and concomitant changes in the protein conformation, may be monitored by the Laue method.

The Laue technique has some inherent difficulties, such as a paucity of low-resolution reflections, overlap of multiple spots, spatial overlap of streaked spots, and an unfavorable peak-to-background ratio (88). These drawbacks result in a requirement for well-diffracting crystals with low mosaic spread. Since success in Laue diffraction experiments is not guaranteed even if good diffraction is obtained under conditions of a monochromatic experiment, evaluation of the quality of the data obtainable by the Laue technique for trigonal crystals of *Tc*AChE was undertaken. The initial goal was to obtain a data set of sufficient quality to permit resolution of structural features within the active site. To test this, crystals were soaked with a solution of a small reversible ligand, edrophonium (EDR) (see Fig. 4). The structure of the complex of *Tc*AChE with EDR was determined earlier using monochromatic radiation (20). Comparison of electron density maps obtained from Laue data with maps obtained from monochromatic data should reveal whether use of the Laue technique is feasible for performing time-resolved studies on AChE.

The monochromatic data set on the *Tc*AChE-EDR complex that was used as a reference for estimating the quality of the Laue data set was obtained from crystals grown in the same way as those for the Laue data set, using PEG200 as a precipitant (56), rather than the ammonium sulfate employed previously (20). The new data were collected at 4°C, at the EMBL outstation of the DESY in Hamburg, Germany, beam line X11, on a 30cm MAR Research IP detector (λ=0.92Å). The crystal had a mosaic spread of 0.29° and diffracted to a resolution of 2.4Å; further details concerning the quality of the data are given in Table 1. The structure obtained from the monochromatic synchrotron data is virtually identical to the previously determined structure with PDB access code 1ACK (20): the r.m.s.d. between coordinates for all Cα atoms is 0.29Å, and a plot of the r.m.s.d. values of the backbone versus residue number does not show any major conformational changes. The r.m.s.d. for the ten non-hydrogen atoms of the ligands is 0.30Å.

Laue data on crystals of *Tc*AChE soaked with EDR were collected at the European Synchrotron Radiation Facility (ESRF) in Grenoble, France, at the white radiation beam line BL3 (ID9), with a wavelength range of 0.4 to 1.5Å. The crystals, mounted in a capillary, were tested at 4°C, using an FTS cooling device. Several crystals had to be discarded due to lack of high-resolution reflections and/or severe streaking of the spots. Good diffraction was obtained from a rather large crystal, 0.5x0.5x0.4 mm^3, that showed a reasonably low mosaicity. 24 still frames with an exposure time of 1 ms and a crystal-to-film distance of 300 mm were collected while rotating the crystal over 5° along the spindle axis between exposures. The data, collected on an X-ray image intensifier coupled to a CCD camera, were corrected, using the package FIT2D (89), for spatial distortions and non-uniformity of response.

The crystal orientation parameters and relative cell dimensions were determined using the program LAUECELL (90). The scaled cell dimensions (a=b=113.0, c=136.8Å) are close to the values found for monochromatic data on non-frozen trigonal *Tc*AChE crystals in general. The program LAUEVIEW (91) was used for further processing of the data. The Laue spots on the patterns were predicted using a resolution-dependent wavelength bandpass, based on a known starting λ–curve and Wilson statistics. Since the distribution of the single spots as a function of the wavelength is not uniform, wavelength normalization was done in two parts (see Fig. 5). The single spots are more densely distributed between 0.45Å (λ_{min}) and 0.9Å ($2\lambda_{min}$) than at wavelengths higher than 0.9Å. The λ–curve for wavelengths between 0.45 and 0.9Å was simulated with a 16-term Chebychev polynomial, and the curve for wavelengths between 0.9 and 1.25Å with a 3-term Chebychev. Fig. 5 also shows a Bragg-angle cut-off (*i.e.* no spots in the upper right corner of the figure): the crystal diffracted beyond the edge of the detector. However, the risk of overlapping spots prevented a significant reduction of the crystal-to-detector distance.

The resolution limit (d_{min}) used for processing the Laue data set is 2.8Å, compared to 2.4Å for the monochromatic data. The combined λ–curve (shown in Fig. 6) was used for deconvolution of the multiples (92); this significantly increased the completeness of the data, especially in the ∞-$2d_{min}$ range.

Details of the quality of the Laue data set are given in Table 2. The amplitudes of the full Laue data set give a correlation of 91.6% with those of corresponding reflections in the monochromatic data set (see Fig. 7); for the singles, the correlation is 93.4% and for the deconvoluted multiples, 87.8%.

The same refinement procedure was used for both the monochromatic and Laue data sets. The coordinates of native *Tc*AChE in the trigonal crystal form (PDB access code 2ACE) were used as a starting model; 5% of the data (1891 reflections for the monochromatic and 1032 for the Laue data) were reserved for use in a test set for cross-validation of the refinement process. To reduce the chance of introducing model bias into the initial maps, the reflections for the test set were taken by selecting the corresponding reflections from the test set used for refinement of the native structure (56). Initial maps were calculated after rigid-body movement of the coordinates for protein residues using the program X-PLOR v. 3.851 (93). The difference between R and R_{free} at this point was 2.6% for the monochromatic and 2.2% for the Laue data, compared to 3.6% for the final stage of refinement of 2ACE without waters. A random test set would have given R and R_{free} of the same value; the obtained differences indicate that most of the model bias has been eliminated. Subsequent refinement was done using the maximum-likelihood refinement procedure of REFMAC (94), using all data between 20.0Å and the highest resolution, and manual model building using O (95). The R-factor (R_{free}) after refinement is 21.3% (25.8%) for the monochromatic and 20.7% (26.8%) for the Laue data. The final model contains 252 waters for the monochromatic structure and 144 for the Laue structure, and the r.m.s. deviation between the two structures is 0.20Å for all Cα atoms.

Obtaining a data set of reasonable quality from Laue diffraction is not a guaranteed success for every crystallized protein. The Laue method has been applied with good results to well-behaving proteins such as cutinase (96), restrictocin (97) and for photoactive yellow protein (98); it has also been applied to crystals of high symmetry, such as tomato bushy stunt virus (99). Since the question of the exit route for reaction products from the active site of AChE had been raised, we had sought a method that would permit us to establish unequivocally whether or not there is a "back door" to the active-site gorge. Laue diffraction, with its extremely short exposure times and high information content per image, could well supply such information, provided that four conditions are met:

- initiation of the enzymatic reaction must be synchronised
- the reaction needs to be on a time scale commensurate with that of data collection
- the existence of intermediate states needs to be ascertained
- the Laue data need to be of adequate quality

Synchronization is currently being investigated using caged compounds especially developed and synthesized for this purpose. The compounds synthesized are nitrobenzyl derivatives of choline and of carbamylcholine (CCh), which generate the corresponding free ligands upon photoactivation (85, 86). Their interaction with *Tc*AChE has been studied both in solution (86), and in the crystal state, using monochromatic crystallography (Raves, unpublished results).

The existence of one intermediate state in the hydrolysis of ACh, the acetylated enzyme, is well known (100). The carbamylated enzyme formed during the hydrolysis of CCh provides a more stable intermediate that should be observable using time-resolved crystallography, because the decarbamylation of the enzyme through hydrolysis is much slower than deacylation (87). However, since the pathway of release of the reaction product of interest, choline, is unknown, the question of whether an intermediate state is involved in the release cannot be answered at this point.

The quality of the Laue data depends on the resolution and completeness attainable, the reliability of the measured intensities, and the interpretability of the electron density maps that follows from these factors.

Unlike in monochromatic diffraction experiments, the high-resolution spots in a Laue image not only have a higher Bragg angle on average, placing them further towards the edge of the detector, they also cause a higher density of spots in all regions of the image. In the case of AChE, where all three unit cell axes are longer than 100Å, and the mosaicity of the crystals is rarely below 0.2°, spatial overlap of spots is problematic. Although the program used for integration, LAUEVIEW (91), is able to deconvolute overlapping reflections to some extent, simulations showed that a serious reduction of the crystal to detector distance (*e.g.* 200 instead of 300 mm) was unlikely to give useful data for these crystals. A theta offset of the detector could, however, have been instrumental in obtaining more unique data, as is indicated by the Bragg cut-off in Fig. 5. Another data collection strategy that could have been beneficial for these crystals was described by Yang *et al.* (97): to reduce the extent of X-ray heating of the crystal by regulating the exposure time. The resolution cut-off that was chosen for the data set described in the previous section was 2.8Å. For the purpose of these studies and the kind of structural changes we hope to see, 2.8Å resolution should be sufficient.

In terms of completeness (see Table 2) the quality of the dataset is very good: 95.2% in the medium resolution range (5.6-3.4Å). The problem of the low-resolution hole (88) has largely been overcome, given the completeness of 82.8% between ∞ and 5.6Å ($2d_{min}$), which stems from the fact that a relatively large number (24) of frames were collected, aided by the powerful deconvolution algorithm of the program that was used for processing the data, LAUEVIEW (91). At higher resolutions, the completeness of the reflections is lower, but adequate for inclusion in the dataset.

The amplitudes of the reflections correlate fairly well with those of the monochromatic data set. From Fig. 7 it can be seen that there is a slight tendency to overestimate weak reflections, but the overall correlation coefficient of 91.6% indicates that the amplitudes are fairly reliable. The R_{sym} of the Laue data set, 14.8% *vs.* 6.5% for the monochromatic data up to 2.8Å, also indicates a reduction of the quality of the data; but is still acceptable given the reduction in total X-ray exposure from several hours to 24 ms. Since the program LAUEVIEW (91) gives the user full manual control of the integration, rejection and scaling criteria, the completeness of the dataset is a trade-off against other parameters which are indicative for the quality of the data. The inclusion of the non-redundant single-observation reflections into the dataset, for example, improved the completeness, but caused some deterioration in the correlation with the monochromatic data. In addition, the determination of the wavelength normalisation curve strongly depends on the accuracy of the intensities, and special care had to be taken not to include too many unreliable measurements, while still being left with as high a redundancy as possible. The final wavelength normalisation curve obtained (Fig. 6) did not show details such as the Pt-edges arising from the focussing mirror (91), but has the correct overall appearance.

Special consideration was given to the problem of model bias in the initial electron density maps, since the structure to be determined from the Laue data is very similar to that of the protein in the native state. For this purpose, the same reflections that were used in the test set in the refinement of the initial starting model (56) were flagged in the monochromatic and Laue data sets of the EDR complex (101). After rigid-body refinement of the entire protein, the difference between R and R_{free} indicates that most of the model bias had been avoided.

Fig. 8 shows a comparison of the Fourier difference maps, after rigid-body refinement of the active-site region, for the Laue data set *vs.* the complete monochromatic data set, and *vs.* the selection of reflections from the monochromatic data set which are present in the Laue data. As is to be expected, the electron density difference maps made using the Laue data are of somewhat lower quality than the ones obtained using the monochromatic data; the signals are weaker, and the maps are noisier and show less detail, reflecting the difference in R_{sym} values and completeness for the two data sets. Nevertheless, the difference map obtained from the Laue data clearly shows the location, the orientation and the shape of the soaked-in inhibitor, EDR.

In addition, a peak search on the initial Laue difference map yielded 78 peaks higher than 3.0 σ that correspond to water molecules in the monochromatic structure, indicating that the maps are interpretable. For some of the incomplete side chains in the initial model (61 atoms in 23 different residues are disordered in the native structure), several could be located in the maps for the monochromatic structure, reducing the number of missing atoms to 57 in 22 residues. The Laue maps showed even more of the missing atoms, leaving only 51 atoms in 19 residues undetermined. It is especially encouraging to observe that the conformational change that Oγ of the active-site S200 undergoes upon binding of EDR (20), from hydrogen-bonding to H440 in the native state to interacting with the oxyanion hole in the complex, is visible in the electron-density maps of the Laue data set (see Fig. 9). Such detailed information will be extremely relevant in the determination of a transient intermediate structure and of structural changes during the enzymatic reaction.

Based on the data presented in this chapter, it has been shown that the Laue technique can be reliably applied to crystals of a protein as large as AChE, in a static state. The maps from a data set of 24 images, with an overall completeness of 84.5% and an R_{sym} (unweighted) of 14.8%, clearly show the position of the ligand inside the active site, and structural changes in important protein residues. This data set does not represent the maximum quality attainable for AChE crystals: use of a theta offset for the detector, and reduction of the extent of X-ray heating of the crystal could improve the useful resolution limit and the reliability of the intensities.

To improve the usefulness of the Laue method for AChE, future studies will concentrate on synchronization of release of the caged compound, and on coordinating data collection with either movement of choline out of the gorge (for the caged choline compound) or with carbamylation and decarbamylation (for the caged CCh).

Structure of the rhAChE/fasciculin complex

Knowledge of the 3D structure of hAChE is of importance for drug design, in particular of anti-Alzheimer drugs (102, 103), for development of improved procedures for treatment of intoxication by nerve agents (6), and for design of safer and more effective insecticides.

Vertebrate AChE occurs as an array of molecular forms which differ in the number of subunits which they contain and in their quaternary structure (104). Recombinant hAChE (rhAChE), expressed in HEK 293 cells, is secreted into the culture medium as a mixture of monomers, dimers and tetramers (105); additional heterogeneity may arise due to variations in the extent of glycosylation (106) and to proteolytic 'nicking'. Such heterogeneity may severely impede crystallization. To alleviate this problem, a mutant of rhAChE was constructed in which the C-terminus had been truncated to give rise to a homogeneous monomeric form (107). The T subunit expressed was devoid of the C-terminal hydrophobic sequence corresponding to residues 544-583, including C580, which forms the interchain disulfide in oligomeric forms (108). These residues were replaced by the pentapeptide, ASEAP, which is the natural C-terminal sequence in the H subunit (104).

Truncation was performed by DNA cassette replacement. Specifically, the 187 bp DNA fragment between *BssHII* and *SalI* in pL5CA was replaced by the synthetic DNA duplex. The truncated DNA sequence was introduced into a tripartite expression vector expressing also the reporter gene *cat* and the selection marker *neo*. The expression vector coding for the expression of monomeric rhAChE was introduced into HEK 293 cells. Stable clones, secreting high levels (> 4 U/ml/h) of truncated enzyme (ΔCter–rhAChE), were isolated and used in large-scale production (109), so as to produce amounts of purified enzyme adequate for crystallization. Purification was carried out by affinity chromatography (16). Analytical sucrose density gradient centrifugation showed, as anticipated, that a homogeneous monomeric species was produced, which migrated slightly more slowly than the WT monomer. SDS-PAGE suggested a similar degree of glyocsylation-related microheterogeneity in the truncated and WT enzymes. The molecular weight of the truncated polypeptide, after removal of sugar side chains by glycanase, is 60kD, as compared to 64kD for the WT polypeptide. This difference in size is as predicted from the difference in chain length of the two forms. Finally, the catalytic characteristics of the truncated enzyme, as well as the inhibition constants for its inhibition both by active and peripheral site ligands, are essentially identical to those for the WT enzyme.

A homologous truncated DNA sequence, in which site-directed mutagenesis afforded expression of the E202Q mutant (31), was generated, expressed and characterized similarly to the WT enzyme.

Both WT rhAChE and the E202Q mutant were cocrystallized as a stoichiometric complex with the polypeptide toxin, fasciculin-II (FAS-II) (110), from the venom of the green mamba, as had previously been done for both *Tc*AChE (79) and mAChE (78). Crystallization of the FAS-II complexes of both WT and E202Q rhAChE, from ammonium sulfate at neutral pH and 19°C, yielded crystals of irregular prism morphology, which grew within 1-3 weeks to 0.01-0.1 mm in size. Recrystallization from water resulted in larger crystals, up to 0.8 mm in size. The crystals exhibited rhombohedral symmetry of space-group R32, with unit cell dimensions a=b=150Å, c=247Å, with a single copy of the complex in the asymmetric unit.

X-ray data were collected on the X12C beamline of the NSLS, at Brookhaven National Laboratory, in both cases from a single cryogenically cooled crystal. The overall completeness of the 30A-2.7Å data is 99.0% and 83.4%, with R_{merge} 8.1% and 9.1%, for WT and E202Q AChE, respectively. For the wild-type enzyme, the current R_{work} is 22% and the R_{free} is 29%, and for the E202Q structure, the corresponding figures are 21 and 24%, respectively. In both structures, the electron density reveals residues 5-490 and 497-543 of the rhAChE polypeptide chain, and all 61 residues of FAS-II. The 490-497 sequence is homologous to the external 485-490 sequence in *Tc*AChE, which is not visible in the native 2ACE structure, but can be seen in the recently refined complex with E2020 (111). In the published mouse structure (PDB ID 1MAH), residues 4-543 are all present; but, judging from the temperature factors, residues 491-499 are poorly determined, especially at the 3.2Å higher resolution limit of this structure. The electron density of the WT rhAChE structure shows the location of ~200 water molecules (none were reported for mAChE); one *N*-glycosylation site, at N350, seen also in the mAChE structure; and additional density near T504, which is a putative *O*-glycosylation site.

Structure solution of the rhAChE/FAS-II complex was carried out by molecular replacement, using the *Tc*AChE /FAS-II structure (PDB ID 1FSS, (79) as a probe molecule and, subsequently, as a starting model for refinement. Diffraction data for the E202Q mutant were refined similarly, but using the rhAChE/FAS-II structure as a starting model. The structures were refined using X-PLOR (simulated annealing (112)) and CNS (simulated annealing coupled with maximum likelihood technique (113)).

Close inspection of the rhAChE/FAS-II structure reveals a high degree of similarity between it and the two other complexes of AChE with FAS-II, *viz.* of *Tc*AChE and mAChE (78, 79), especially in the active-site region and within the aromatic gorge. Small variations can be found in some loops and in the insertion/deletion regions. Our results validate use of *Tc*AChE as a model for gaining a general understanding of the structure of AChE. However, they also paved the way for a study of the subtle differences in structure which may account for species-dependent differences in specificity for substrates and inhibitors. Such subtle differences must be taken into account in design of drugs, *e.g.* for treatment of Alzheimer patients, for treatment of nerve gas intoxication, and in producing insecticides with a high degree of selectivity for insect vs. human AChE.

Residue E202, which is adjacent to the active-site serine, S203(*200)*, is one of three charged residues at the bottom of the active-site gorge, and plays an important role in AChE reactivity. Yet, the 3D structure of the E202(*199*)Q mutant is almost identical to that of the WT enzyme. The reduction in catalytic efficiency displayed by the E202Q mutant, either toward charged or uncharged substrates, and the marked concomitant decreases in rates of both phosphylation and aging (31, 114), was explained by the participation of residue E202(*199*) in the chemical process involving the catalytic triad residue H447(*440*) (115). It was proposed earlier that E202(*199*) plays a key role in maintaining a network of H-bonds that span the cross-section of the active-site gorge

(114). The role suggested for this network is to stabilize the functional architecture of the active center, and to ensure proper positioning of E202(*199*), thereby stabilizing acylation and phosphylation transition states. Central to this array are the two water molecules bridging residues E202(*199*)-E450(*443*) and E202(*199*)-Y133(*131*). Indeed, replacement of any of these three residues reduces catalytic activity to a similar degree (31). The two water molecules appear to be conserved in the E202Q mutant. Replacement of E202 by D leads to an even greater decrease in enzymatic activity. Despite the fact that the charge in E202D is maintained, these data suggest that the H-bond network is disrupted due to the shorter side chain of D202. It will be of interest to investigate whether the H-bond network involving the water molecules is maintained in the E202D mutant.

Homology modeling of AChE and related proteins

The concept of an electrostatic motif on the surface of biological macromolecules as a definite topographical pattern of electrostatic potentials in 3D space, provides a powerful tool for identification of functionally important regions on the surface of structurally related macromolecules (116). This pattern can only be defined in the context of molecules of similar 3D structure, for only in such a case is it possible to unambiguously orient the motif with respect to zones of the related macromolecules which might be functionally significant. We have used this approach to localize a functional region common to ChEs and to a set of neural cell-adhesion proteins, which include gliotactin (GLI) (117), neurotactin (NRT) (118) and neuroligin (NL) (119). It has been suggested that these adhesion proteins are structurally related to ChEs due to their high sequence similarity (120); however, they lack the active-site serine.

The high degree of identity among AChE and BChE sequences has permitted construction of homology models of the 3D structures of BChE (33) and of AChE from different species (121). Examination of the 3D structure of *Tc*AChE showed the enzyme to be characterized by a marked asymmetric spatial distribution of charged residues; the charges were shown to roughly segregate into a 'northern' negative hemisphere (taking the mouth of the gorge as the north pole) and a 'southern' positive one (73). This electrostatic pattern was shown to give rise to a large dipole moment which was calculated to be ~1600 Debyes, oriented roughly along the axis of the active-site gorge (73, 74, 122). Electro-optical measures performed on AChE from *Bungarus fasciatus* gave a value of ~1000 Debye, thus confirming experimentally the order of magnitude of the macrodipole (123).

The asymmetric distribution of surface potentials was thought to be essential for the fast catalysis effected by ChEs. This assumption has been reevaluated in the light of site-directed mutagenesis experiments on rhAChE in which up to seven charged residues in the vicinity of the entrance to the active-site gorge were neutralized. The ensuing drastic reduction of the asymmetric distribution of surface potentials did not have a major effect on catalysis (124). Brownian dynamics simulations of bimolecular rate association constants for ACh and AChE also failed to show a meaningful correlation between the distribution of electrostatic surface potentials and catalysis (125). A further analysis of the electrostatic properties of the 3D structures and homology models of ChEs, aimed at generating a detailed and quantitative topographical map of the electrostatic surface potentials, identified the presence of an "annular" electrostatic motif of negative surface potential around the entrance of the active-site gorge (121). The role of surface potentials in catalysis is not clear-cut. It has been shown to play only a minor role in the case of isozymes of trypsin differing by as much as 12.5 charge units. The catalytic efficiency of these isozymes was shown to be influenced not by electrostatic surface potentials, but by a few charged amino acids localized close to the active site (126). These considerations drove us to investigate whether the role of surface potentials in ChE might be related to roles other than catalysis.

ChEs possess a 3D fold different from those of "classical" serine hydrolases, such as chymotrypsin and subtilisin. This fold is called the α/β hydrolase fold (127), and has been shown to characterize a family of hydrolytic enzymes of widely different phylogenetic origin and substrate specificity. Some of these enzymes, like the fungal triacylglycerol lipases from *Geotrichum candidum* and *Candida rugosa* (128), show substantial sequence similarity with ChEs. Other members of the family, like haloalkane halogenase from *Xenobacter autotrophicus* and dienelactone hydrolase from *Pseudomonas* sp., do not show significant sequence similarity to the ChEs; but inspection of their 3D structures shows that their polypeptide chain has the structural core typical of the α/β hydrolase fold (127). A systematic search of sequence databases has retrieved a large number of proteins with a high degree of sequence similarity to α/β hydrolases (120). Inspection of the sequences reveals that amongst an overwhelming majority of enzymes, there are also a few proteins involved in cell adhesion; these contain a ChE-like domain whose function is most probably independent of hydrolase activity since the active-site serine is mutated to a glycine. Amongst them are the three proteins which we chose to investigate, because of their presumed involvement in cell adhesion and signaling in the nervous system.

GLI is a transmembrane protein transiently expressed on peripheral glia of *Drosophila melanogaster* embryos and required for formation of the peripheral blood-nerve barrier (117). The C-terminal extracellular domain of this protein shows substantial sequence similarity with ChEs. Such similarity can also be found in the extracellular domain of NRT, a transmembrane glycoprotein which is expressed in neuronal and epithelial tissues during embryonic and larval stages (118, 129). Sequence similarities suggest that neuroligins (NLs), a family of mammalian neuronal cell surface protein that act as ligands for β-neurexins (119), also contain an extracellular ChE-like domain. NLs and neurexins mediate interactions between neurons and contribute to the specific organization of synapses. Both the *Drosophila* adhesion proteins and NL are involved in heterophilic cell-cell interactions, suggesting that their ChE-like domains possess a recognition function that has been conserved from invertebrates to vertebrates. It is worth noticing that both GLI and NRT display susbstantially higher sequence similarity with *Tc*AChE than with the *Dm*AChE enzyme (Table 3), and that the targets of their adhesive functions have not yet been identified.

The sequence similarity between ChEs, NL, GLI, and NRT prompted us to build homology models of their extracellular domains, both to confirm the presence of shared structural motifs and to investigate the possibility that they might display similar electrostatic characteristics. Our underlying assumption is that the ChE-like domains of these adhesion proteins are independently folded, and that neither their conformation nor their electrostatic properties will be greatly affected by the association with the non-ChE like regions of GLI, NL and NRT, which are mostly transmembrane and intracellular (Fig. 10).

The homology models were built with the automated knowledge-based building tool Swiss-Model (130), and validated as described previously (121). The same modelling procedure was applied as a control to the neutral lipase from *G. candidum* (*Gc*Lip) (131), whose 3D structure is known, to check for the bias in modelling introduced by the templates. The modelling of *Gc*Lip gave a structure very close to the actual 3D structure solved by X-ray crystallography (α-carbon RMS deviation ~1.1Å from the 3D X-ray structure of *Gc*Lip). Since all the proteins involved in this study possess about the same degree of sequence identity as *Gc*Lip does with *Tc*AChE (see Table

3), we can reasonably assume our models to be close approximations of the actual structures of these domains.

The electrostatic surface potentials of *Tc*AChE (PDB entry 2ACE), GLI, NL, and NRT were calculated solving the Poisson-Boltzmann equation by the finite difference method (FDPB) (132), using the DelPhi algorithm (133) as implemented in the GRASP program (134). As a control, we examined the distribution of surface potentials for other members of the α/β hydrolase family to check whether the "annular" electrostatic motif was a characteristic shared by most members of this family. We chose three enzymes with a sequence identity to ChEs similar to that of NL, NRT and GLI. The three enzymes selected were cholesterol esterase from *Candida rugosa* (135) (*Cr*CE, PDB entry 1CLE), *Gc*Lip (PDB entry 1THG) and bile-salt-stimulated lipase from rat (rBSSL) (136). In this last case the 3D structure is not yet available, and a homology model was built following the same procedure used for GLI, NRT and NL. We also calculated the surface potentials for hBChE, for hAChE and for the mutant of rhAChE in which seven negatively charged residues near the entrance of the gorge had been neutralized (7-hAChE). The structures of 7-hAChE, NL, NRT GLI, *Gc*Lip, *Cr*CE and rBSSL were superimposed on that of *Tc*AChE by a least-squares fitting procedure implemented in the program LSQMAN (137), and placed in a common orientation in which the axis of the active-site gorge of *Tc*AChE (as defined by Antosiewicz *et al.* (122)) is aligned with the cartesian Z-axis.

Our most significant result is shown in Fig. 11. It is immediately apparent that the electrostatic surface potential contours of *Tc*AChE, GLI, NRT and NL are strikingly similar. All three proteins show a characteristic "annular" electrostatic motif of negative potential around the zone homologous to the active-site gorge of the ChEs. In contrast, *Gc*Lip, rBSSL, and *Cr*CE appear to display a different topographical distribution of surface potentials (Fig. 11a). In the case of the 7-hAChE mutant, neutralization of seven negatively charged residues in the "annular" region virtually erases the electrostatic motif, while not affecting the negative potential gradient within the active-site gorge. This distribution of electrostatic surface potentials is very similar to that of hBChE (Fig. 11b). This finding correlates well with the contention that the potential gradient inside the active-site gorge makes a more important contribution to ChE catalysis than the surface potentials around the rim of active-site gorge (124, 138).

In order to provide a quantitative measure of the electrostatic motif of the molecules studied, we calculated the average surface potential over a 20Å wide region of accessible surface around the zone homologous to the entrance of the active-site gorge of *Tc*AChE (which constitutes the common Z axis). This region was divided into 1Å wide concentric sections, and the average potentials in the sections were plotted and correlated by a linear regression fit with the results obtained for *Tc*AChE (see Table 4, Fig. 12). GLI, NRT and NL are all characterized by a high correlation coefficient and an average potential in the "annular" region very similar to that of *Tc*AChE; in addition, their potential gradient closely follows that of *Tc*AChE. Of the three lipases, only *Cr*CE shows a high correlation coefficient and an average potential similar to AChE, but its RMS deviation from the ChE-like fold is the largest amongst all the proteins examined, and its potential gradient is substantially different from that of *Tc*AChE. It is of interest that BChE displays a lower average potential in the “annular” region and a very poor correlation coefficient, in addition to a potential gradient similar to that of the lipases.

The biological significance of the electrostatic surface potential of ChEs has been the subject of speculations, and it has been proposed that it might have a non-catalytic function (124).There is mounting evidence that ChEs may be involved in functions distinct from their catalytic activity. During development of the nervous system of vertebrates, expression of ChEs is associated with periods of enhanced neurite outgrowth (139, 140), suggesting that they might serve as neuronal growth factors or cell-adhesion molecules. It has been speculated that the site responsible for the non-catalytic interaction of ChEs is localized close to the entrance of the active-site gorge, possibly overlapping with what has been termed the “peripheral” anionic site (PAS) of AChE, a possible locus of regulation of enzymatic activity (27, 30, 141), which is located in the region of the “annular” electrostatic motif. In a recent study, AChE was shown to promote neurite regeneration in cultured adult neurons of the mollusk *Aplysia* (142). The growth-promoting action of AChE was shown to be independent of its catalytic function. Inhibition of the active site did not influence the neurotrophic action of AChE, but occupancy of its PAS suppressed neurite regeneration (142). There is also evidence that the PAS of AChE can enhance the rate of formation of amyloid fibrils, a major component of the senile plaques found in the brains of Alzheimer patients (143). Strong evidence for a common recognition mechanism in cell-adhesion between ChEs, GLI and NLs comes from a recent study, in which chimeric constructs of the C-terminal transmembrane domain of NRT, fused to the extracellular ChE-like domains of *Dm*AChE or *Tc*AChE, were shown to be endowed with the same heterophilic adhesion properties as wild type NRT (144).

Electrostatic complementarity between interacting proteins has been found to be one of the major driving forces for complex formation (145). Mutagenesis and electrostatic screening studies of the association rates between barnase, a ribonuclease, and barstar, its inhibitor, have shown the limiting step to be the formation of a binding transition state, in which the two proteins form a low-affinity non-specific complex held together by long-range electrostatic interactions (146). We speculate that a possible mechanism effected by the “annular” motif might be the facilitation of target recognition via low specificity associations mediated by long-range electrostatic interactions with a pool of ligands displaying a complementary motif, followed by a subsequent docking step with the unique functional ligand(s), to yield the final high affinity complex. Some support for our hypothesis comes from the mode of binding of AChE to one of its strongest inhibitors, fasciculin II (FAS), a three-fingered polypeptide toxin from the venom of the green mamba (110). These polypeptide snake venom toxins constitute a family of 6-8 kDa proteins, of which α-bungarotoxin, a potent antagonist for the nicotinic ACh receptor, is the best known member.

FAS has been shown to bind in a “cork-and-bottle fashion” to the entrance of the active-site gorge of AChE, which is situated in the negatively charged “northern” hemisphere (78, 79). The surface complementarity between enzyme and inhibitor is very large; about 2000Å^2 of accessible surface are buried upon binding, including the region of the “annular” motif. In addition to this large surface complementarity, the AChE-FAS complex displays significant electrostatic complementarity. Analysis of the topography of surface potentials of FAS shows that it also possess a "bipolar" motif, with a preponderance of positive surface which is absent in other three-fingered snake toxins (110). This positive surface characterizes the zone of interaction between FAS and AChE (79).

Analysis of the sequence alignment of the proteins which we investigated shows no sequence motif shared exclusively by AChE, GLI, NRT and NL. Thus the conjunction of the topographical distribution of surface potentials with the topological arrangement of the polypeptide chain seems the most important common structural factor conserved between these proteins. It is thus plausible that the shared electrostatic motif indicates a common recognition mechanism or even a common ligand. We hypothesize that a chimeric construct of the cytoplasmic domain of NRT with the mutant form of AChE, in which seven negative residues have been neutralized to abolish the electrostatic motif, will not display the same adhesive properties as a construct built with wild-type AChE. We further predict that constructs with BChE and *Cr*CE will not be able to promote heterogeneous cell adhesion, the former because it lacks the "annular" motif, and the latter because of a large deviation from the common ChE-like fold.

The above considerations lead us to conclude that GLI, NRT, NLs and AChE are the first members of a class of adhesion proteins that, because of their common electrostatic and structural motif, we have decided to name "electrotactins".

Studies on human paraoxonase

Human paraoxonase/arylesterase (PON1) is an esterase with broad substrate specificity. It catalyzes the hydrolysis of paraoxon, and a number of other OPs, and of esters such as phenylacetate. OPs are widely used as insecticides and nerve gases, and are lethal for many species, including humans, due to their inhibition of the synaptic enzyme, AChE, as well as of other esterases and proteases. It has been shown that serum paraoxonase plays a significant role in the detoxification of a variety of OPs in mammals. Furthermore, correlations have been found between the levels of serum paraoxonase and systemic diseases, such as systemic amyloidosis (see BACKGROUND). The enzyme does not correspond to any of the protein sequences in the Swiss-Prot data base or in the protein sequences derived from the GENEBANK database; thus it is difficult to infer any structural information from proteins found in the Brookhaven Protein Data Bank (PDB) (147). Although PON1 may be involved in breakdown of oxidized lipids (BACKGROUND), its physiological role and natural substrate remain to be clearly defined. Structural data may shed light on this issue, and may also offer a new structural motif.

Expression of PON1 has been achieved, both in human 293 kidney cells and in CHO-K1 cells. These expression systems were utilized, in conjunction with site-directed mutagenesis, to obtain evidence for a role in the catalytic action of PON1 of various candidate amino acids, and in an attempt to increase its catalytic efficacy (148, 149). In order to obtain the large quantities of pure protein necessary for X-ray crystallographic studies, both of wild type PON1 and of pertinent mutant forms of the enzyme, we have chosen the Baculovirus (Bac) expression system in insect cells. This expression system has proved itself in recent years to be an extremely versatile and cost effective tool for large scale production of many eukaryotic proteins, with yields of as much as 50mg/l of culture medium (150). A scan of the PDB retrieved almost 100 structures of protein which had been expressed using the Bac expression system (http://www.pdb.bnl.gov). The Bac system has also been successfully used in expression of both wild-type and selenomethionyl variants of human choriogonadotropin (151). The production of selenomethionyl variants of a particular protein is an extremely powerful tool which permits determination of a structure by multiple anomalous diffraction (MAD) techniques (152). This technique requires only a single crystal, with the phase problem being solved by varying the wavelength during data collection. This is in contrast to multiple isomorphous replacement methods, which require crystals that are isomorphous to the native ones with heavy atoms soaked in.

The Bac-based system is a eukaryotic expression system; it thus uses many of the protein modification, processing, and transport systems present in higher eukaryotic cells. Bac is a large, enveloped double-stranded DNA virus that infects arthropods. The viral genome is large (130 kbp); hence it can accommodate large segments of foreign DNA. Viruses enter the cell by adsorptive endocytosis and move to the nucleus, where their DNA is released. Two types of viral progeny are produced: extracellular virus is released from the cell by budding, starting ~12 hr postinfection, and is produced at a logarithmic rate until 20 hr postinfection, after which production falls off. Polyhedra-derived virus, appears in the nucleus at ~18 hr postinfection, and continues to accumulate as late as 72 hr postinfection, or until the cells lyse. Occluded viral particles are embedded in proteinaceous viral occlusions called polyhedra within the nuclei of infected cells. The polyhedrin protein (29 kDa) is the major protein component of the occlusion bodies.

The Bac expression system takes advantage of several properties of the polyhedrin protein: (1) It is expressed at very high levels in infected cells, constituting more than half of the total cellular protein late in the infectious cycle ; (2) It is not essential for infection or replication of the virus; (3) Viruses lacking the polyhedrin gene have a plaque morphology distinct from that of viruses containing the gene. Thus recombinant Bac is engineered to express the desired protein by replacing the polyhedrin gene with a foreign gene coding for this protein through homologous recombination. This is achieved by contransfecting a linearized Bac genome with a transfer vector containing the gene of interest. This transfer vector, besides the elements needed for amplification in *E. coli*, contains a multiple cloning site for the insertion of the target gene, a promoter for the polyhedrin gene and a large tract of Bac genome flanking the cloning region to facilitate homologous recombination. Subsequently, recombinant viruses in which expression of polyhedrin has been replaced by the target protein can be selected by several screening methods. Many commercial improvements to this basic protocol, that report increased efficiency in the produttion of recombinant virus, are available on the market, thus minimizing the time needed for production of a suitable virus.

We have received, from the laboratory of Bert La Du (Department of Pharmacology, University of Michigan), with whom we are collaborating, a variant of the PON1 gene in which residues H19 and Q20 have both been mutated to Ala. This construct permits secretion of PON1 into the medium, by enabling the cell machinery to cleave the N-terminal signal peptide (153). While the resulting product displays reduced activity, its solubility properties are greatly enhanced and we feel that it will constitute an ideal candidate for structural studies. Production of recombinant PON1 will be monitored using antibodies supplied by the La Du laboratory.

In preparatory experiments, performed in our laboratory, the PON1 clone received from the La Du laboratory has been amplified via PCR, in a BlueScript® shuttle vector, with primers designed to contain the appropriate restriction sites for unidirectional cloning in the transfer vector. A region coding for six histidine residues (His-tag) was included in the 3' primer, in order to permit purification of the expressed protein on a nickel column (154). The product was sequenced so as to confirm the integrity of the coding sequence, and to check whether PCR had introduced any errors. The gene fragment was then isolated by digestion with the appropriate restriction enzymes, purified and cloned in an appropriate transfer vector for the Bac expression system, *viz.* AcNPV (155). The initial attempts to express PON1 in Bac will be performed in the next few weeks.

TABLES

Table 1. Monochromatic diffraction data statistics for TcAChE-edrophonium complex

No. of frames	66
Oscillation angle	0.75°
Cell parameters ($P3_121$)	a=b=112.41Å, c=136.55Å
Mosaicity	0.29°
No. of observations	275,832
Unique reflections	38,611
Overall redundancy (highest resolution shell*)	3.1 (3.1)
R_{sym} (highest resolution shell)	8.9% (42.0%)
Average I / average σ (highest resolution shell)	14.0 (2.1)
Completeness (highest resolution shell*)	97.7% (99.6%)

*highest resolution shell: 2.46 - 2.40Å

Table 2. Laue X-ray diffraction data statistics for TcAChE-edrophonium complex

No. of frames	24		
Exposure time	1 ms		
Cell parameters ($P3_121$)	a=b=113.00Å, c=136.80Å		
Singles			
No. of observations*	83,171		
Unique reflections	19,613		
Overall redundancy	4.2		
R_{sym}			
Unweighted	14.8%		
Weighted	10.8%		
Singles and multiples combined			
No. of deconvoluted multiples	5,464		
Total No. of unique reflections	21,122		
Resolution (Å)	Completeness† (%)		R_{sym} (%)
	Shell	Cumulative	
∞ - 11.2	42.0	42.0	14.7
11.2 - 8.4	77.6	62.7	13.0
8.4 - 5.6	91.2	82.8	12.8
5.6 - 4.0	95.1	90.6	13.5
4.0 - 3.4	95.3	92.4	15.2
3.4 - 3.0	87.3	90.4	21.3
3.0 - 2.8	61.3	84.5	25.0

*After rejection of weak spots and those with negative intensity ($I/\sigma(I) < 0.1$), high background, bad profile fitting, and/or bad merging

† Completeness by resolution shell for singles and multiples combined.

Table 3. Sequence identity and similarity between electrotactins, lipases & ChEs

Protein	Percent identity to *Tc*AChE *(DmAChE)*	Percent similarity to *Tc*AChE *(DmAChE)*
Cholinesterases		
*Tc*AChE	100.0	100.0
hAChE	57.6	85.0
mAChE	59.0	85.3
*Dm*AChE	36.3	65.8
7-hAChE	57.6	85.0
hBChE	52.4	83.1
Adhesion proteins		
NRT (*Drosophila*)	31.1 *(25.1)*	57.7 *(50.4)*
GLI (*Drosophila*)	30.6 *(23.5)*	61.0 *(55.7)*
NL (mouse)	32.3	60.1
Lipases		
*Gc*Lip	29.4	56.8
rBSSL	31.2	61.4
*Cr*CE	31.9	56.8

Percent sequence identity and similarity between electrotactins, lipases and ChEs, as given by the BestFit algorithm from the GCG package (version 9, Genetics Computer Group, 575 Science Drive, Madison, WI 53711, USA).The values are calculated with respect to the sequence of *Tc*AChE.

Table 4. Structural deviation between electrotactins, lipases and ChEs

Protein	RMS deviation (Å) of Cα atoms relative to *Tc*AChE (% of matched residues)	Average surface potentials (kT/e) in the "annular" motif region	Correlation coefficients for surface potentials in concentric sections of the "annular" motif region
Cholinesterases			
*Tc*AChE	0.00 (100)	-2.272	1.00
hAChE	0.48 (97.9)	-1.139	0.89
mAChE	0.31 (97.1)	-1.409	0.80
*Dm*AChE	0.77 (98.1)	-2.358	0.86
7-hAChE	0.48 (97.9)	-0.052	0.90
hBChE	0.42 (94.9)	-0.724	0.66
Adhesion proteins			
Nrt (*Drosophila*)	1.19 (94.7)	-2.132	0.83
Gli (*Drosophila*)	1.12 (86.5)	-1.194	0.94
NL (mouse)	1.10 (84.6)	-1.332	0.89
Lipases			
*Gc*Lip	1.46 (64.4)	-0.551	-0.45
rBSSL	0.85 (93.0)	-0.020	0.59
*Cr*CE	1.54 (71.5)	-1.571	0.89

RMS structural deviation (Å) of the Cα atoms, average surface potentials (kT/e) and correlation coefficients for electrostatic surface potentials between electrotactins, lipases and ChEs. The values are calculated with respect to the 3D structure and electrostatic properties of *Tc*AChE.

FIGURES

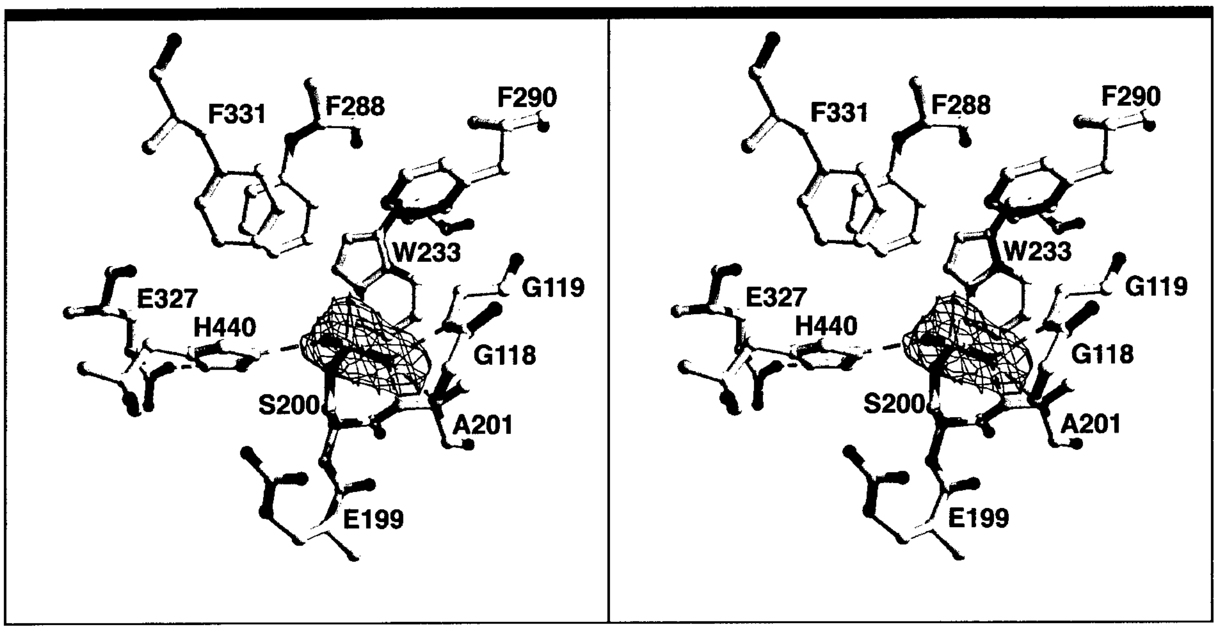

Fig 1. Difference Fourier map of the 'aged' soman-TcAChE conjugate

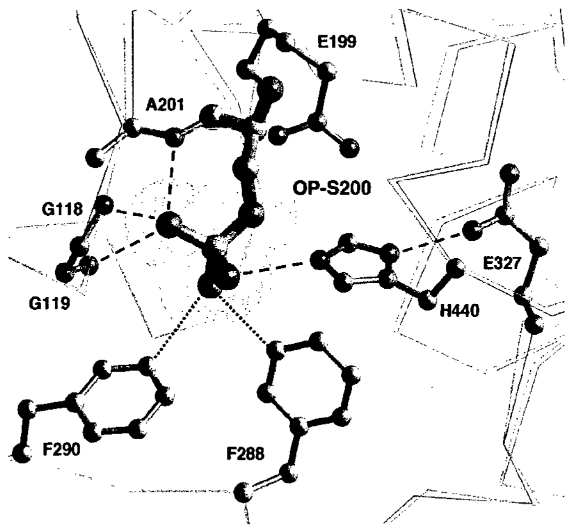

Fig.2. Active site of MeP-TcAChE, obtained by reaction with sarin

Note the proximity of four H-bond donors (dashed lines) to the anionic phosphonyl oxygen atoms: *viz* the backbone amide nitrogens of A201, G118, and G119, and Nε2 of H440. The OP methyl carbon is within non-bonded contact distances (dotted lines) of F288 (3.6Å to Cε1) and F290 (3.6Å to Cε1) in the acyl pocket. For reference, the Cα-traces of native- and OP-enzyme are overlaid. The active site shown is essentially identical to that obtained with soman (not shown), except for minor differences in inter-atomic distances.

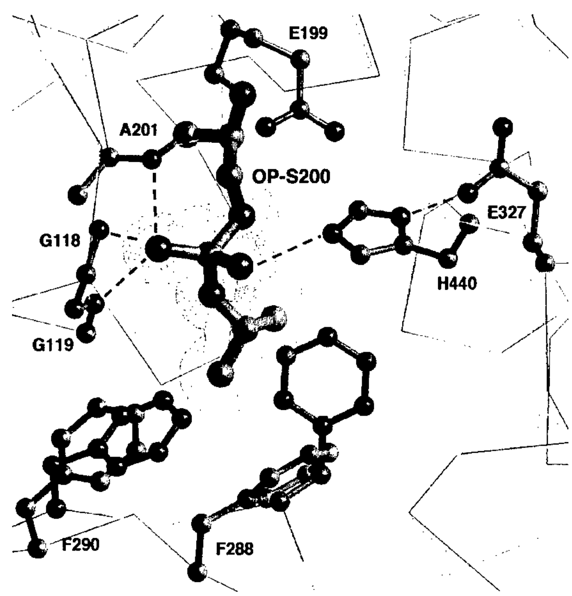

Fig.3. Active site of MiPrP-TcAChE obtained by reaction with DFP

As with aged phosphonylated AChE, the stability of M*i*PrP-AChE apparently stems from four potential H-bond donors (dashed lines) to the anionic phosphoryl oxygen atoms. However, unlike for soman or sarin, the reaction with DFP results in a distortion of the main chain in the acyl pocket of AChE. F288 and F290 move significantly from their positions in the native enzyme (shown with thin dark lines for reference). The Cα- traces of native- and M*i*PrP-*Tc*AChE are overlaid.

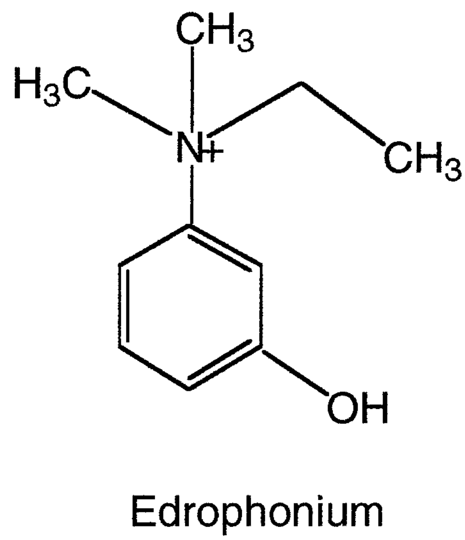

Fig.4. Structure of edrophonium

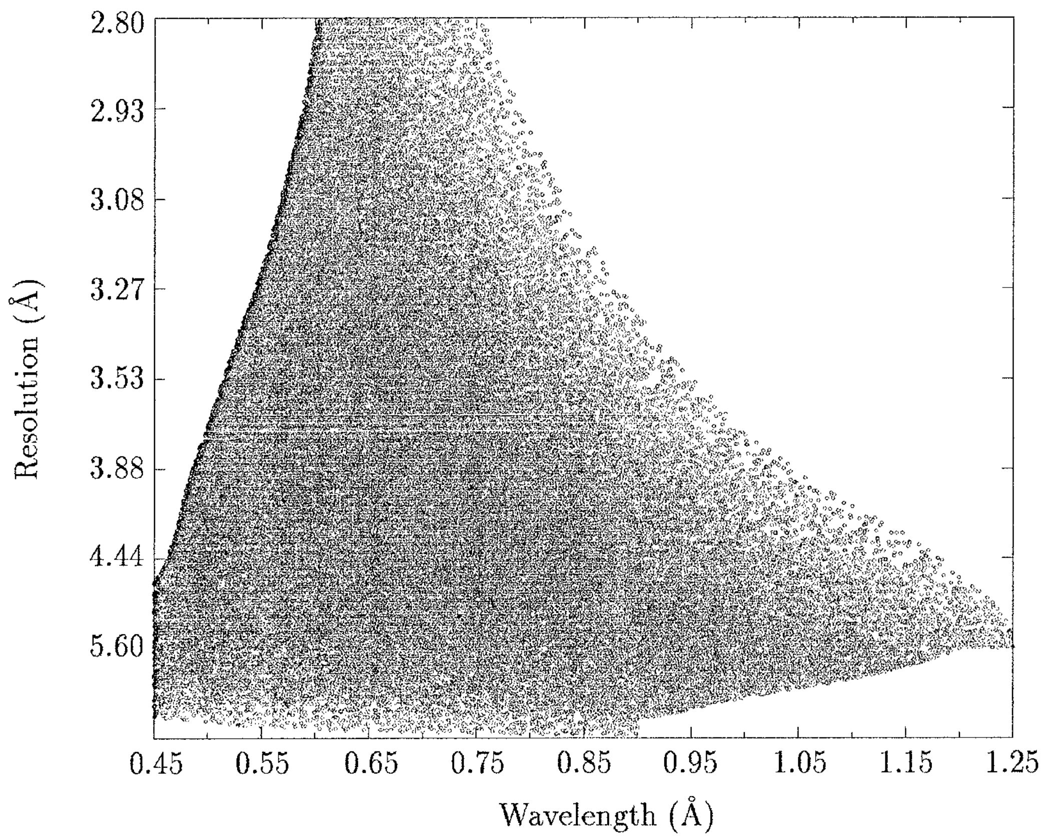

Fig.5. Distribution of single reflections: resolution versus wavelength

The Bragg-angle cut-off is clearly seen at higher wavelengths and higher resolution.

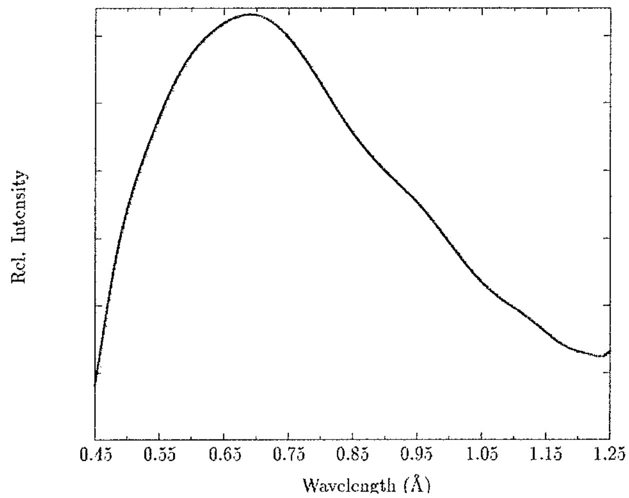

Fig.6. Normalization curve for ID9, ESRF, deduced from the Laue data set for TcAChE

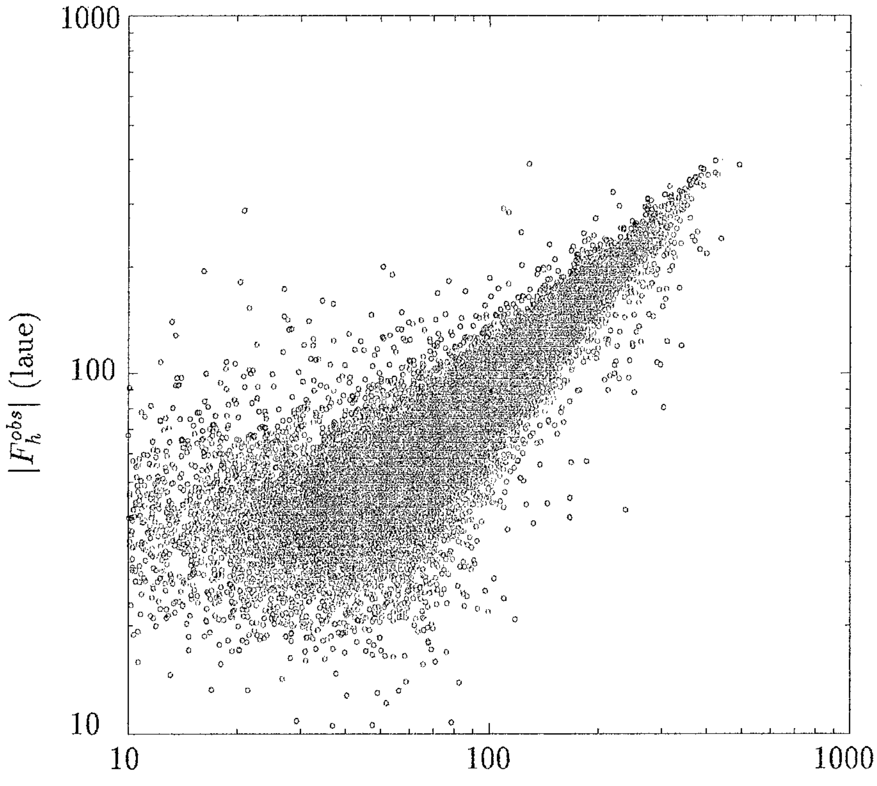

Fig.7. Correlation between Laue and monochromatic structure-factor amplitudes

The correlation is 91.6%, based on 19,725 unique reflections that were observed in both data sets.

Fig.8. Difference electron density maps for the EDR in the EDR/TcAChE complex

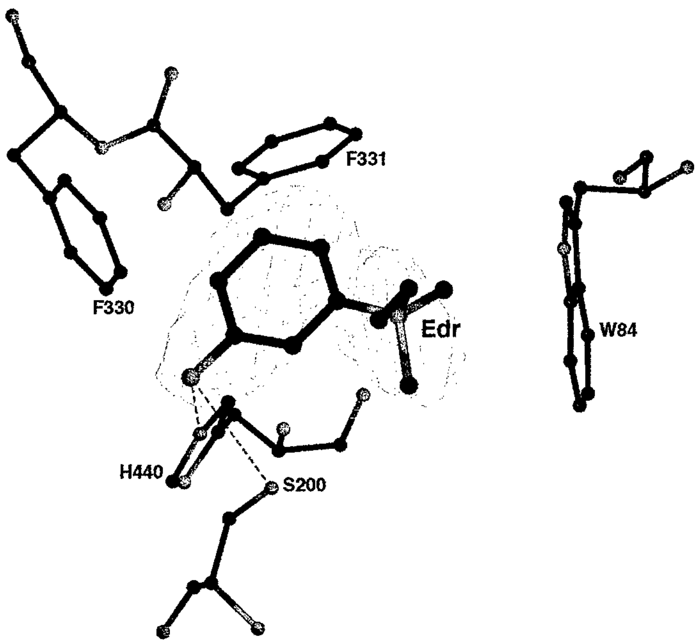

8a) All monochromatic data to 2.4Å. The ligand is emphasized with larger balls and sticks. F^{obs}-F^{calc} maps at 3.5 σ cut-off are shown in green; only electron density around the ligand is shown.

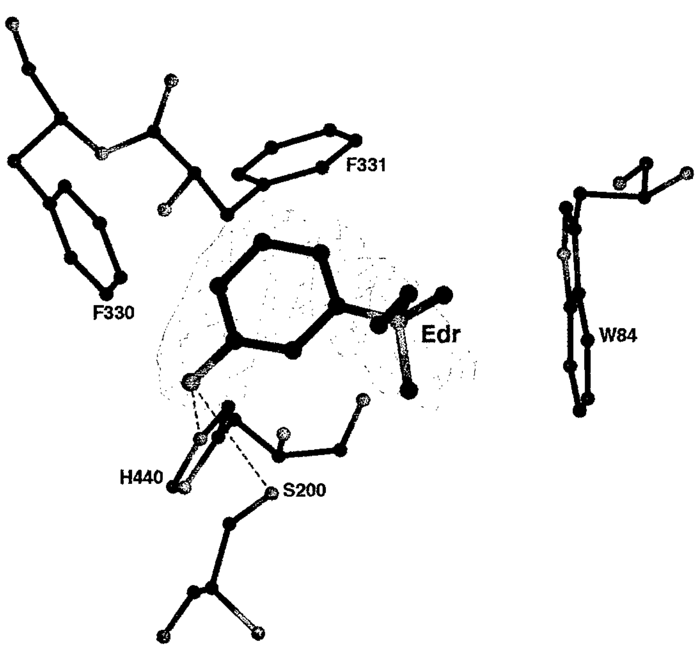

8b) Selected monochromatic reflections which are also present in the Laue data set (2.8Å). Representation as in Fig. 8a.

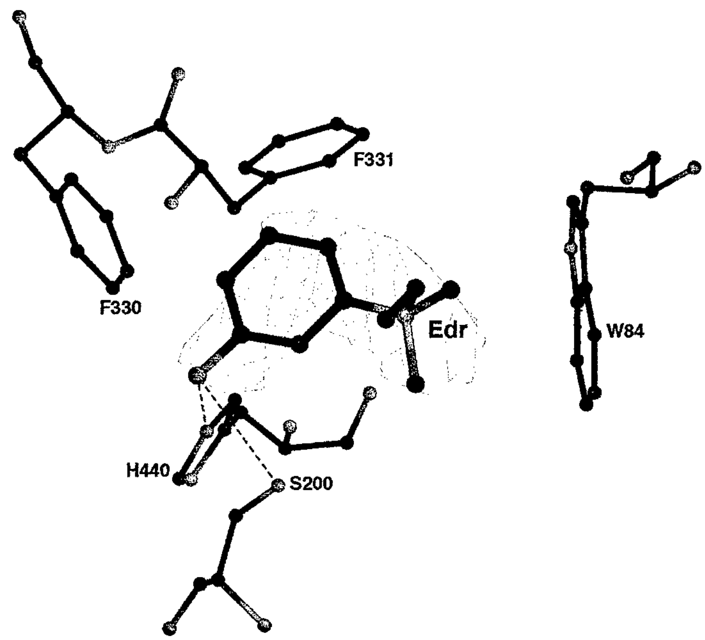

8c) Laue data (2.8Å), Representation as in Fig. 8a.

Fig.9. Conformational change in S200 produced upon binding of edrophonium

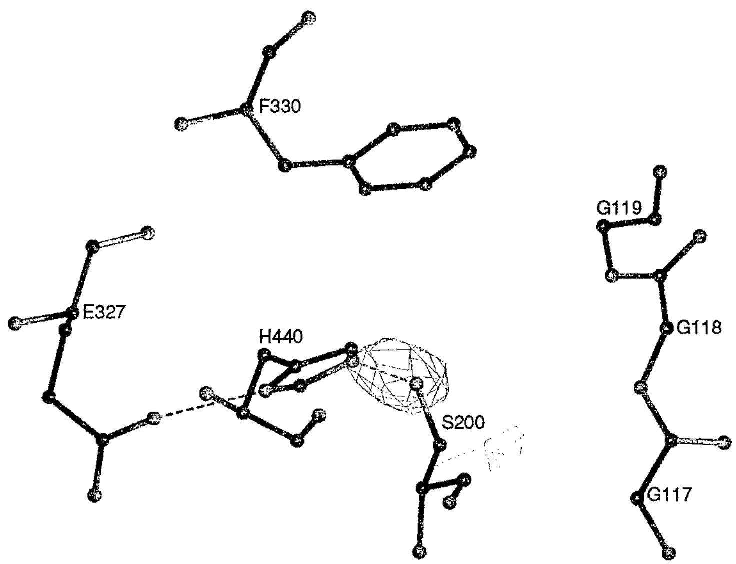

9a) Difference electron density maps from the Laue data directly after rigid-body refinement.
F^{obs}-F^{calc} maps, drawn in the vicinity of Ser200, are contoured at 2.7 and -2.7 σ cut-off, and shown in green and red, respectively. Protein residues in the native structure are shown in black.

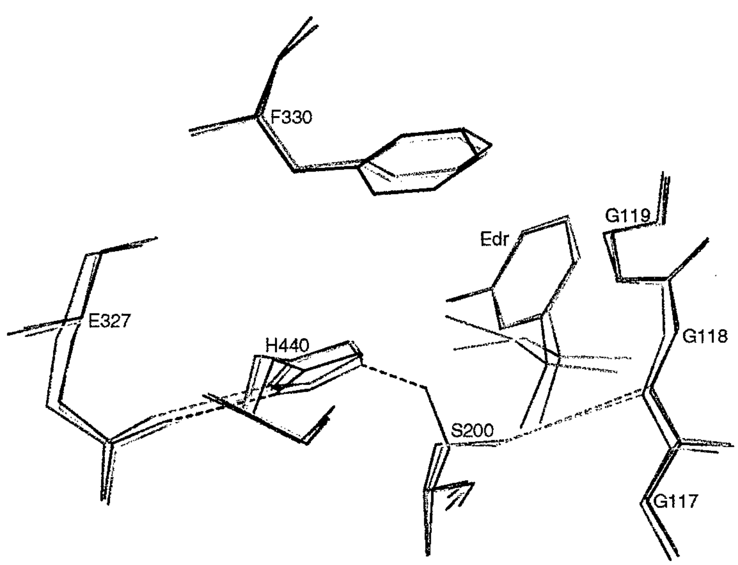

9b) Stick model of (i) the native starting model (shown in black); (ii) refined model using monochromatic data (shown in green); (iii) refined model using Laue data (shown in gold).

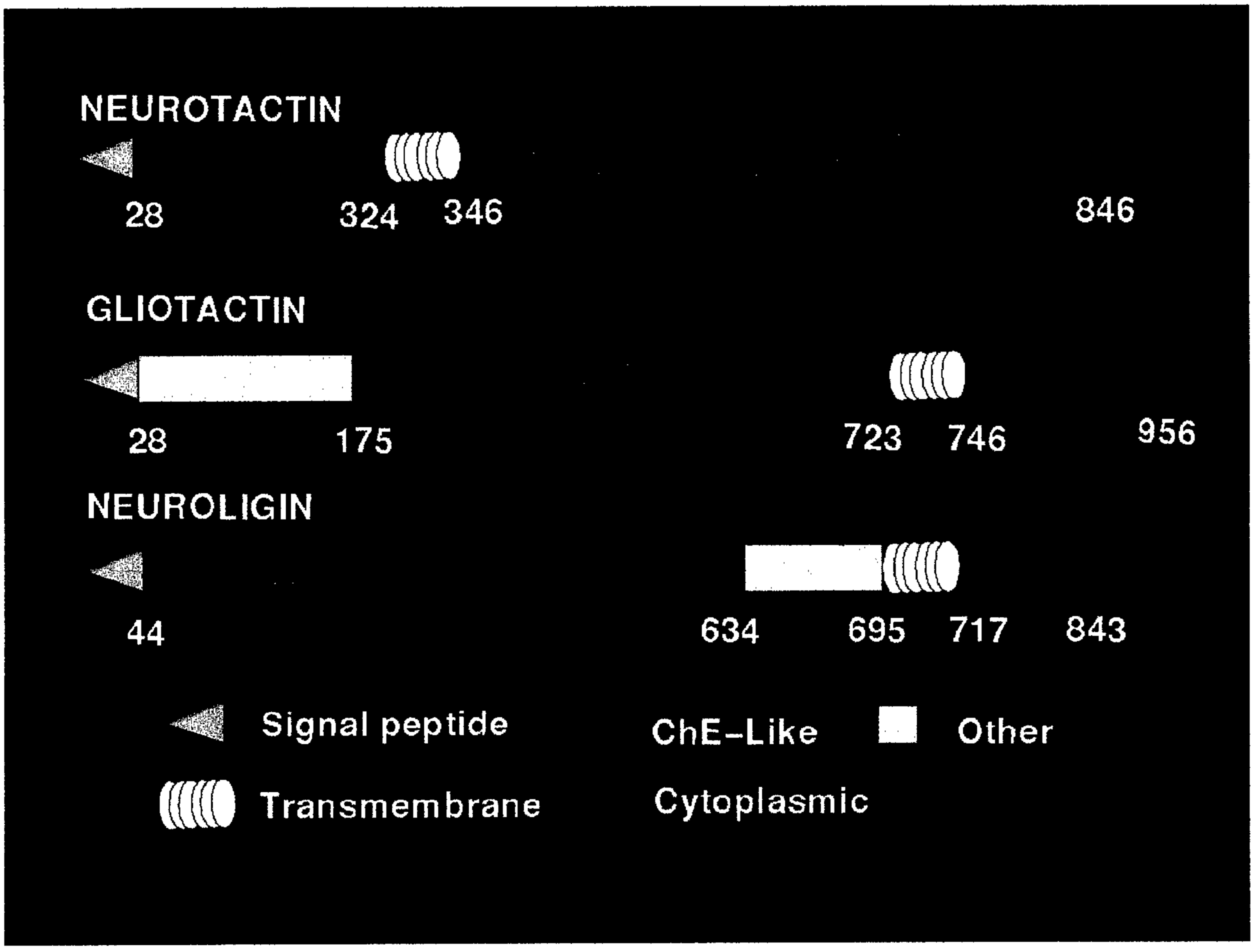

Fig.10. Schematic representations of domain organizations of GLI, NRT & NL

Fig.11. GRASP image of electrostatic surface potentials in electrotactins & lipases

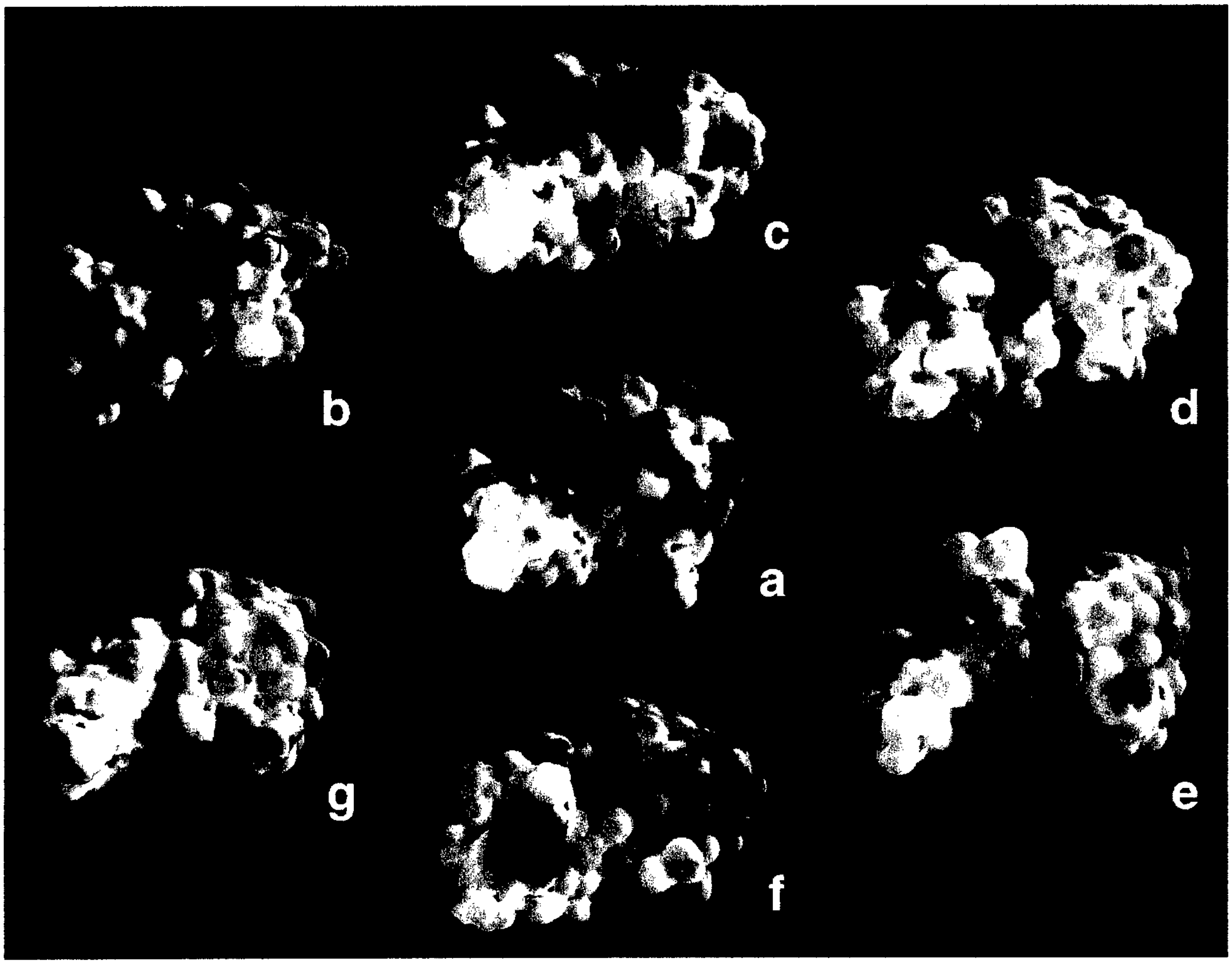

11a) (a) *Tc*AChE; (b) NRT; (c) NL; (d) GLI; (e) *Cr*CE; (f) rBSSL; (g) *Gc*Lip. The presence of the "annular" electrostatic motif in the adhesion molecules and in AChE should be noted. The values of surface potentials are expressed as a spectrum ranging from +0.25*kT/e* (deep blue) through 0 *kT/e* (white) to -0.25 *kT/e* (deep red). At a temperature of 298.15 K, *kT/e* = 25.7 mV. The surface potentials are calculated for a salt concentration of 0.145 M, with a cubic grid of linear dimensions of 65Å, a protein dielectric constant of 4 and a solvent dielectric constant of 78.

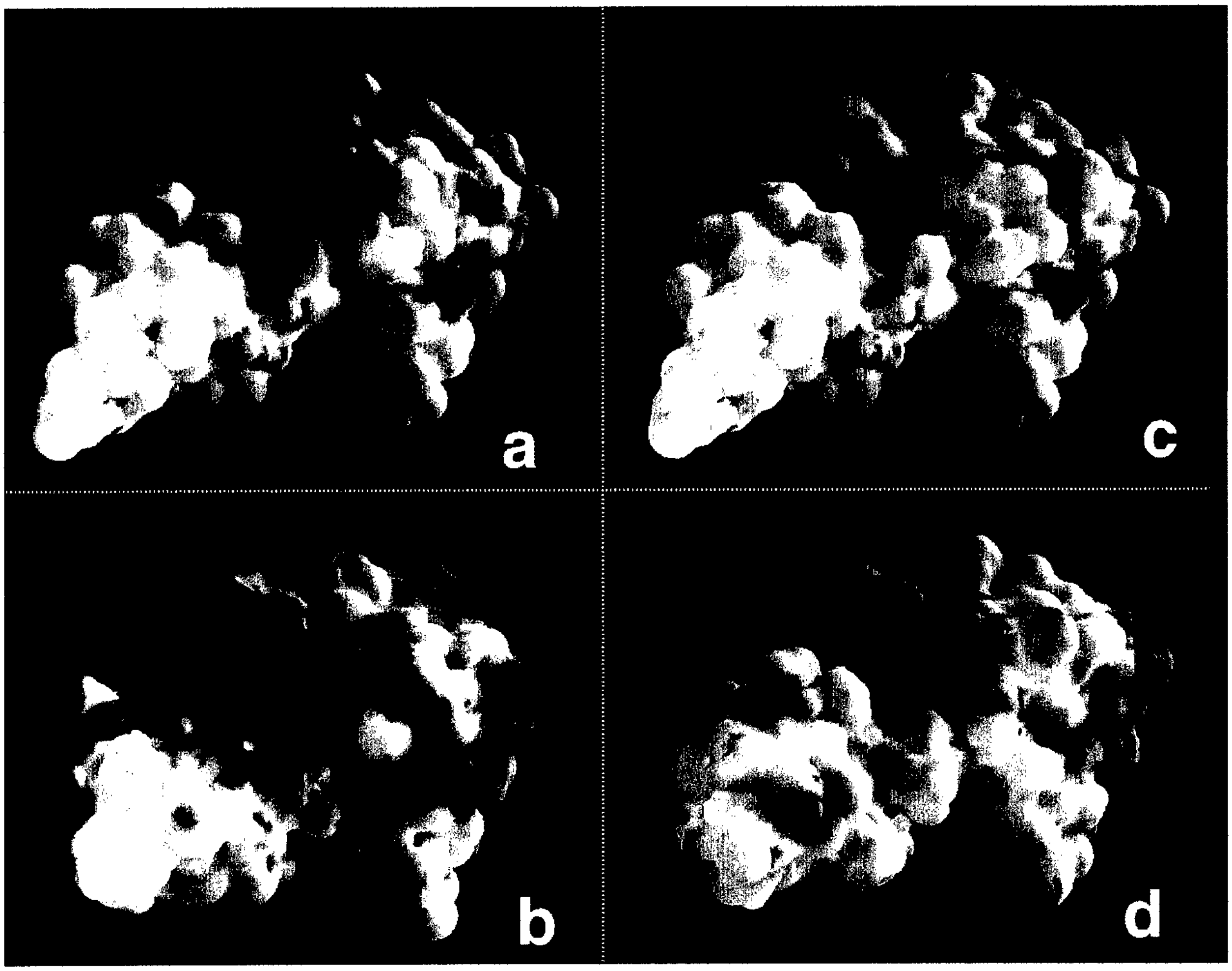

11b) (a) hAChE; (b) *Tc*AChE; (c) 7-hAChE; (d) hBChE, showing the absence of the "annular" motif in hBChE and its neutralization in the 7-hAChE mutant.

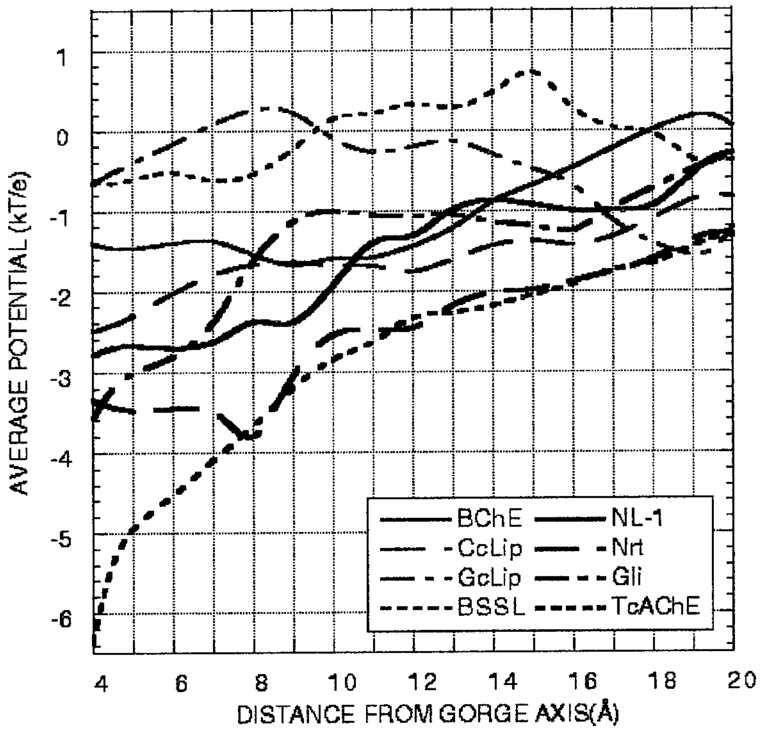

Fig.12. Plots of average surface potentials measured in concentric "annular" sections.

The plots show the change in average potential perpendicular to the gorge axis, in the "annular" motif region, for hBChE, *Cr*CE, *Gc*Lip, BSSL, NL, NRT, GLI and *Tc*AChE. The origin is placed on the axis of the active-site gorge of *Tc*AChE (122), and the potential values are expressed in units of kT/e, where k is Boltzmann's constant, T the temperature in K, and e the electronic charge. At a temperature of 298.15 K, kT/e = 25.7 mV.

REFERENCES:

1. Neuromuscular transmission - enzymatic destruction of acetylcholine (1974), Barnard, E. A., In *The Peripheral Nervous System* (J.I. Hubbard, Eds.), pp. 201-224, Plenum, New York.

2. Acetylcholinesterase: Enzyme structure, reaction dynamics, and virtual transition states (1987), Quinn, D. M., *Chem. Rev.*, **87**, 955-975.

3. Kinetics of acetylthiocholine binding to electric eel acetylcholinesterase in glycerol/water solvents of increased viscosity. Evidence for a diffusion-controlled reaction (1982), Hasinoff, B. B., *Biochim. Biophys. Acta*, **704**, 52-58.

4. Fractional diffusion-limited component of reactions catalyzed by acetylcholinesterase (1986), Bazelyansky, M., Robey, C. and Kirsch, J. F., *Biochemistry*, **25**, 125-130.

5. *Cholinesterase and Anticholinesterase Agents* (1963), Koelle, G. B., Eds., Springer-Verlag, Heidelberg.

6. Anticholinesterases: medical applications of neurochemical principles (1995), Millard, C. B. and Broomfield, C. A., *J. Neurochem.*, **64**, 1909-1918.

7. *Enzyme Inhibitors as Substrates: Interactions of Esterases with Esters of Organophosphorus and Carbamic Acids* (1972), Aldridge, W. N. and Reiner, E., North-Holland Publishing, Amsterdam.

8. Anticholinesterase agents (1990), Taylor, P., In *The Pharmacological Basis of Therapeutics, 5th edition* (A.G. Gilman, A.S. Nies, T.W. Rall and P. Taylor, Eds.), pp. 131-150, MacMillan, New York.

9. *Cholinergic basis for Alzheimer therapy* (1991), Becker, R. E. and Giacobini, E., Eds., Birkhäuser, Boston.

10. *Alzheimer Disease: Therapeutic Strategies* (1994), Giacobini, E. and Becker, R., Eds., Birkhäuser, Boston.

11. Tacrine: an overview of efficacy in two parallel group studies (1994), Gracon, S. I. and Knapp, M. J., In *Alzheimer Disease: Therapeutic Strategies* (E. Giacobini and R. Becker, Eds.), pp. 145-149, Birkhäuser, Boston.

12. Donepezil approved for treatment of Alzheimer's disease (1997), Nightingale, S. L., *JAMA*, **277**, 10.

13. Acetylcholine binding by a synthetic receptor: implications for biological recognition (1990), Dougherty, D. A. and Stauffer, D. A., *Science*, **250**, 1558-1560.

14. Acetylcholinesterase: structure and use as a model for specific cation-protein interactions (1992), Sussman, J. L. and Silman, I., *Curr. Opin. Struct. Biol.*, **2**, 721-729.

15. Nicotinic acetylcholine receptor at 9 Å resolution (1993), Unwin, N., *J. Mol. Biol.*, **229**, 1101-1124.

16. Purification and crystallization of a dimeric form of acetylcholinesterase from *Torpedo californica* subsequent to solubilization with phosphatidylinositol-specific phospholipase C (1988), Sussman, J. L., Harel, M., Frolow, F., Varon, L., Toker, L., Futerman, A. H. and Silman, I., *J. Mol. Biol.*, **203**, 821-823.

17. Atomic structure of acetylcholinesterase from *Torpedo californica*: a prototypic acetylcholine-binding protein (1991), Sussman, J. L., Harel, M., Frolow, F., Oefner, C., Goldman, A., Toker, L. and Silman, I., *Science*, **253**, 872-879.

18. Structure and dynamics of the active site gorge of acetylcholinesterase: synergistic use of molecular dynamics simulation and X-ray crystallography (1994), Axelsen, P. H., Harel, M., Silman, I. and Sussman, J. L., *Protein Sci.*, **3**, 188-197.

19. Effective charge on acetylcholinesterase active sites determined from the ionic strength dependence of association rate constants with cationic ligands (1980), Nolte, H.-J., Rosenberry, T. L. and Neumann, E., *Biochemistry*, **19**, 3705-3711.

20. Quaternary ligand binding to aromatic residues in the active-site gorge of acetylcholinesterase (1993), Harel, M., Schalk, I., Ehret-Sabatier, L., Bouet, F., Goeldner, M., Hirth, C., Axelsen, P., Silman, I. and Sussman, J. L., *Proc. Natl. Acad. Sci. USA*, **90**, 9031-9035.

21. The X-ray structure of a transition state analog complex reveals the molecular origins of the catalytic power and substrate specificity of acetylcholinesterase (1996), Harel, M., Quinn, D. M., Nair, H. K., Silman, I. and Sussman, J. L., *J. Am. Chem. Soc.*, **118**, 2340-2346.

22. Alignment of amino acid sequences of acetylcholinesterases and butyrylcholinesterases (1991), Gentry, M. K. and Doctor, B. P., In *Cholinesterases: Structure, Function, Mechanism, Genetics and Cell Biology* (J. Massoulié, F. Bacou, E. Barnard, A. Chatonnet, B.P. Doctor and D.M. Quinn, Eds.), pp. 394-398, American Chemical Society, Washington, DC.

23. A model of butyrylcholinesterase based on the X-ray structure of acetylcholinesterase indicates differences in specificity (1992), Harel, M., Silman, I. and Sussman, J. L., In *Multidisciplinary Approaches to Cholinesterase Functions* (A. Shafferman and B. Velan, Eds.), pp. 189-194, Plenum Press, New York.

24. The inhibitory effect of stilbamidine, curare and related compounds and its relationship to the active groups of acetylcholine esterase. Action of stilbamidine upon nerve impulse conduction (1950), Bergmann, F., Wilson, I. B. and Nachmansohn, D., *Biochim. Biophys. Acta*, **6**, 217-224.

25. Ligand binding properties of acetylcholinesterase determined with fluorescent probes (1974), Mooser, G. and Sigman, D. S., *Biochemistry*, **13**, 2299-2307.

26. Interaction of fluorescence probes with acetylcholinesterase. The site and specificity of propidium binding (1975), Taylor, P. and Lappi, S., *Biochemistry*, **14**, 1989-1997.

27. Role of the peripheral anionic site on acetylcholinesterase: inhibition by substrates and coumarin derivatives (1991), Radic, Z., Reiner, E. and Taylor, P., *Mol. Pharmacol.*, **39**, 98-104.

28. Three distinct domains distinguish between acetylcholinesterase and butyrylcholinesterase substrate and inhibitor specificities (1993), Radic, Z., Pickering, N., Vellom, D. C., Camp, S. and Taylor, P., *FASEB J.*, **7**, A1067.

29. Dissection of the human acetylcholinesterase active center - determinants of substrate specificity - identification of residues constituting the anionic site, the hydrophobic site, and the acyl pocket

(1993), Ordentlich, A., Barak, D., Kronman, C., Flashner, Y., Leitner, M., Segall, Y., Ariel, N., Cohen, S., Velan, B. and Shafferman, A., *J. Biol. Chem.*, **268**, 17083-17095.

30. Differential effects of "peripheral" site ligands on *Torpedo* and chicken acetylcholinesterase (1994), Eichler, J., Anselmet, A., Sussman, J. L., Massoulié, J. and Silman, I., *Mol. Pharmacol.*, **45**, 335-340.

31. Substrate inhibition of acetylcholinesterase: residues affecting signal transduction from the surface to the catalytic center (1992), Shafferman, A., Velan, B., Ordentlich, A., Kronman, C., Grosfeld, H., Leitner, M., Flashner, Y., Cohen, S., Barak, D. and Ariel, N., *EMBO J.*, **11**, 3561-3568.

32. Modelling and mutagenesis of butyrylcholinesterase based on the X-ray structure of acetylcholinesterase (1992), Silman, I., Harel, M., Krejci, E., Bon, S., Chanal, P., Sussman, J. L. and Massoulié, J., In *Membrane Proteins: Structures, Interactions and Models* (A. Pullman, J. Jortner and B. Pullman, Eds.), pp. 177-184, Kluwer Academic Publishers, Dordrecht, Holland.

33. Conversion of acetylcholinesterase to butyrylcholinesterase: modeling and mutagenesis (1992), Harel, M., Sussman, J. L., Krejci, E., Bon, S., Chanal, P., Massoulié, J. and Silman, I., *Proc. Natl. Acad. Sci. USA*, **89**, 10827-10831.

34. Compilation of evaluated mutants of cholinesterases (1995), Shafferman, A., Kronman, C. and Ordentlich, A., In *Enzymes of the Cholinesterase Family* (A.L. Balasubramanian, B.P. Doctor, P. Taylor and D.M. Quinn, Eds.), pp. 481-488, Plenum Press, New York.

35. Three distinct domains in the cholinesterase molecule confer selectivity for acetyl- and butyrylcholinesterase inhibitors (1993), Radic, Z., Pickering, N. A., Vellom, D. C., Camp, S. and Taylor, P., *Biochemistry*, **32**, 12074-12084.

36. Amino acid residues controlling acetylcholinesterase and butyrylcholinesterase specificity (1993), Vellom, D. C., Radic, Z., Li, Y., Pickering, N. A., Camp, S. and Taylor, P., *Biochemistry*, **32**, 12-17.

37. Serum esterases II. An enzyme hydrolysing diethyl *p*-nitrophenyl acetate (E600) and its identity with the A-esterase of mammalian sera (1953), Aldridge, W. N., *Biochem. J.*, **53**, 117-124.

38. Paraoxon hydrolysis vs. covalent binding in the elimination of paraoxon in the rabbit (1986), Butler, E. G., Eckerson, H. W. and La Du, B. N., *Drug Metab. Dispos.*, **13**, 640-645.

39. Mice lacking serum paraoxonase are susceptible to organophosphate toxicity and atherosclerosis. (1998), Shih, D. M., Gu, L., Xia, Y. R., Navab, M., Li, W. F., Hama, S., Castellani, L. W., Furlong, C. E., Costa, L. G., Fogelman, A. M. and Lusis, A. J., *Nature*, **394**, 284-287.

40. *Enzymes Hydrolyzing Organophosphorus Compounds* (1989), Reiner, E., Aldridge, W. N. and Hoskin, F. C. G., Eds., Ellis Horwood, Chichester.

41. *Enzymes Interacting with Organophosphorus Compounds* (1993), Reiner, E. and Lotti, M., Eds., Elsevier, Shannon.

42. Purification of a DFP-hydrolyzing enzyme from squid head ganglion (1972), Hoskin, F. C. G. and Long, R. J., *Arch. Biochem. Biophys.*, **150**, 548-555.

43. Purification and properties of the phosphotriesterase from *Pseudomonas diminuta* (1989), Dumas, D. P., Caldwell, S. R., Wild, J. R. and Raushel, F. M., *J. Biol. Chem.*, **264**, 19659-19665.

44. Human serum paraoxonase/arylesterase (1992), La Du, B. N., In *Genetic Factors Influencing the Metabolism of Foreign Compounds* (W. Kalow, Eds.), pp. 51-91, Pergamon, New York.

45. Three-dimensional structure of phosphotriesterase: an enzyme capable of detoxifying organophosphate nerve agents (1994), Benning, M. M., Kuo, J. M., Raushel, F. M. and Holden, H. M., *Biochemistry*, **33**, 15001-15007.

46. Three-dimensional structure of the binuclear metal center of phosphotriesterase (1995), Benning, M. M., Kuo, J. M., Raushel, F. M. and Holden, H. M., *Biochemistry*, **34**, 7973-7978.

47. Characterization of the zinc binding site of bacterial phosphotriesterase (1992), Omburo, G. A., Kuo, J. M., Mullins, L. S. and Raushel, F. M., *J. Biol. Chem.*, **267**, 13278-13283.

48. Structural characterization of the divalent cation sites of bacterial phosphotriesterase by ^{113}Cd NMR spectroscopy (1993), Omburo, G. A., Mullins, L. S. and Raushel, F. M., *Biochemistry*, **32**, 9148-9155.

49. The human serum paraoxonase/arylesterase polymorphism (1983), Eckerson, H. W., Wyte, C. M. and La Du, B. N., *Am. J. Hum. Genet.*, **35**, 1126-1138.

50. Serum paraoxonase status: a major factor in determining resistance to organophosphates (1993), Li, W. F., Costa, L. G. and Furlong, C. E., *J. Toxicol. Environ. Health*, **40**, 337-346.

51. Purification of human serum paraoxonase/arylesterase: evidence for one esterase catalyzing both activities (1991), Gan, K. N., Smolen, A., Eckerson, H. W. and La Du, B. N., *Drug Metab. Dispos.*, **19**, 100-106.

52. Molecular basis for the polymorphic forms of human serum paraoxonase/arylesterase: glutamine or arginine at position 191, for the respective A or B allozymes (1993), Adkins, S., Gan, K. N., Mody, M. and La Du, B. N., *Am. J. Hum. Genet.*, **52**, 598-608.

53. The molecular basis of the human serum paraoxonase activity polymorphism (1993), Humbert, R., Adler, D. A., Disteche, C. M., Hassett, C., Omiecinski, C. J. and Furlong, C. E., *Nat. Genet.*, **3**, 73-76.

54. Characteristics of the genetically determined polymorphic forms of human serum paraoxonase/arylesterase (1991), Smolen, A., Eckerson, H. W., Gan, K., Hailat, N. and La Du, B. N., *Drug Metab. Dispos.*, **19**, 107-112.

55. Studies on human serum paraoxonase/arylesterase (1993), La Du, B. N., Adkins, S., Kuo, C.-L. and Lipsig, D., *Chem. Biol. Interactions*, (in press).

56. 3D structure of acetylcholinesterase complexed with the nootropic alkaloid, (-)-huperzine A (1997), Raves, M. L., Harel, M., Pang, Y.-P., Silman, I., Kozikowski, A. P. and Sussman, J. L., *Nature Struct. Biol.*, **4**, 57-63.

57. Nerve agent stereoisomers: analysis, isolation, and toxicology (1988), Benschop, H. P. and de Jong, L. P. A., *Acc. Chem. Res.*, **21**, 368-374.

58. Origins and diversity of the aging reaction in phosphonate adducts of serine hydrolase enzymes: What characteristics of the active site do they probe? (1995), Bencsura, A., Enyedy, I. and Kovach, I. M., *Biochemistry*, **1995**, 8989-8999.

59. Why nature chose phosphates (1987), Westheimer, F. H., *Science*, **235**, 1173-1178.

60. Direct observation and elucidation of the structures of aged and nonaged phosphorylated cholinesterases by ^{31}P NMR spectroscopy (1993), Segall, Y., Waysbort, D., Barak, D., Ariel, N., Doctor, B. P., Grunwald, J. and Ashani, Y., *Biochemistry*, **32**, 13441-13450.

61. The structure of bovine trypsin: electron density maps of the inhibited enzyme at 5Å and 2.7Å resolution (1974), Stroud, R. M., Kay, L. M. and Dickerson, R. E., *J. Mol. Biol.*, **83**, 185-208.

62. Direct determination of the protonation states of aspartic acid-102 and histidine-57 in the tetrahedral intermediate of the serine proteases: neutron structure of trypsin (1981), Kossiakoff, A. A. and Spencer, S. A., *Biochemistry*, **20**, 6462-6474.

63. Refined crystal structures of "aged" and "non-aged" organophosphoryl conjugates of γ-chymotrypsin (1991), Harel, M., Su, C. T., Frolow, F., Ashani, Y., Silman, I. and Sussman, J. L., *J. Mol. Biol.*, **221**, 909-918.

64. Are the organophosphorous inhibitors of acetylcholinesterase transition-state analogs? (1981), Ashani, Y. and Green, B. S., In *Chemical Approaches to Understanding Enzyme Catalysis: Biomimetic Chemistry and Transition State Analogs* (B.S. Green, Y. Ashani and D. Chipman, Eds.), pp. 169-188, Elsevier, Amsterdam.

65. Serine proteases: Structure and mechanism of catalysis (1977), Kraut, J., *Ann. Rev. Biochem.*, **46**, 331-358.

66. Stereochemical aspects of cholinesterase catalysis (1984), Jarv, J., *Bioorg. Chem.*, **12**, 259-278.

67. Hydrophobic areas on the active surface of cholinesterases (1970), Kabachnik, M. I., Brestkin, A. P., Godovikov, N. N., Michelson, M. J., Rozengart, E. V. and Rozengart, V. I., *Pharmacol. Rev.*, **22**, 355-388.

68. Measurement of the affinity and phosphorylation constants governing irreversible inhibition of cholinesterases by diisopropyl phosphorofluoridate (1966), Main, A. R. and Iverson, F., *Biochem. J.*, **100**, 525-531.

69. The architecture of human acetylcholinesterase active center probed by interactions with selected organophosphate inhibitors (1996), Ordentlich, A., Barak, D., Kronman, C., Ariel, N., Segall, Y., Velan, B. and Shafferman, A., *J. Biol. Chem.*, **271**, 11953-11962.

70. Novel pyrene containing organophosphates as fluorescent probes for studying aging-induced conformational changes in organophosphate-inhibited acetylcholinesterase (1982), Amitai, G., Ashani, Y., Gafni, A. and Silman, I., *Biochemistry*, **21**, 2060-2069.

71. Raman spectroscopic study of conjugates of butyrylcholinesterase with organophosphates (1995), Aslanian, D., Grof, P., Renault, F. and Masson, P., *Biochim. Biophys. Acta*, **1249**, 37-44.

72. Conformational differences between aged and nonaged pyrenebutyl-containing organophosphoryl conjugates of chymotrypsin as detected by optical spectroscopy (1989), Steinberg, N., van der Drift, A. C. M., Grunwald, J., Segall, Y., Shirin, E., Haas, E., Ashani, Y. and Silman, I., *Biochemistry*, **28**, 1248-1253.

73. An electrostatic mechanism for substrate guidance down the aromatic gorge of acetylcholinesterase (1993), Ripoll, D. R., Faerman, C. H., Axelsen, P., Silman, I. and Sussman, J. L., *Proc. Natl. Acad. Sci. USA*, **90**, 5128-5132.

74. Acetylcholinesterase: electrostatic steering increases the rate of ligand binding (1993), Tan, R. C., Truong, T. N., McCammon, J. A. and Sussman, J. L., *Biochemistry*, **32**, 401-403.

75. Open "back door" in a molecular dynamics simulation of acetylcholinesterase (1994), Gilson, M. K., Straatsma, T. P., McCammon, J. A., Ripoll, D. R., Faerman, C. H., Axelsen, P., Silman, I. and Sussman, J. L., *Science*, **263**, 1276-1278.

76. Site-directed mutants designed to test back-door hypotheses of acetylcholinesterase function (1996), Faerman, C., Ripoll, D., Bon, S., Le Feuvre, Y., Morel, N., Massoulié, J., Sussman, J. L. and Silman, I., *FEBS Lett.*, **386**, 65-71.

77. Two conformational states of *Candida rugosa* lipase (1994), Grochulski, P., Li, Y., Schrag, J. D. and Cygler, M., *Protein Sci.*, **3**, 82-91.

78. Acetylcholinesterase inhibition by fasciculin: crystal structure of the complex (1995), Bourne, Y., Taylor, P. and Marchot, P., *Cell*, **83**, 503-512.

79. Crystal structure of an acetylcholinesterase-fasciculin complex: interaction of a three-fingered toxin from snake venom with its target (1995), Harel, M., Kleywegt, G. J., Ravelli, R. B. G., Silman, I. and Sussman, J. L., *Structure*, **3**, 1355-1366.

80. Binding of ^{125}I-fasciculin to rat brain acetylcholinesterase. The complex still binds diisopropyl fluorophosphate (1993), Marchot, P., Khélif, A., Ji, Y. H., Mansuelle, P. and Bougis, P. E., *J. Biol. Chem.*, **268**, 12458-12467.

81. The "back door" hypothesis for product clearance in acetylcholinesterase challenged by site-directed mutagenesis (1994), Kronman, C., Ordentlich, A., Barak, D., Velan, B. and Shafferman, A., *J. Biol. Chem.*, **269**, 27819-27822.

82. Time resolved X-ray structural studies on H-ras p21; identification of the conformational change induced by GTP hydrolysis (1990), Schlichting, I., Almos, S. C., Rapp, G., Wilson, K. S., Petratos, K., Lentfer, A., Wittinghofer, A., Kabsch, W., Pai, E. F., Petsko, G. A. and Goody, R. S., *Nature*, **345**, 309-315.

83. Mutagenesis and Laue structures of enzyme intermediates: isocitrate dehydrogenase (1995), Bolduc, J. M., Dyer, D. H., Scott, W. G., Singer, P., Sweet, R. M., Koshland, D. E. and Stoddard, B. L., *Science*, **268**, 1312-1318.

84. Photolysis of the carbon monoxide complex of myoglobin: nanosecond time-resolved crystallography (1996), Srajer, V., Teng, T., Ursby, T., Pradervand, C., Ren, Z., Adachi, S., Schildkamp, W., Bourgeois, D., Wulff, M. and Moffat, K., *Science*, **274**, 1726-1729.

85. Synthesis and characterization of photolabile choline precursors as reversible inhibitors of cholinesterases: release of choline in the microsecond time-range (1996), Peng, L. and Goeldner, M., *J. Org. Chem.*, **61**, 185-191.

86. Biochemical evaluation of photolabile precursors of choline and carbamoylcholine for potential time-resolved crystallographic studies on cholinesterases (1996), Peng, L., Silman, I., Sussman, J. L. and Goeldner, M., *Biochemistry*, **35**, 10854-10861.

87. Carbamylation of acetylcholinesterase (1960), Wilson, I. B., Hatch, M. A. and Ginsburg, S., *J. Biol. Chem.*, **235**, 2312-2315.

88. On the limitations of the Laue method when applied to crystals of macromolecules (1991), Hajdu, J., Almo, S. C., Farber, J. K., Petsko, G. A., Wakatsuki, S., Clifton, I. J. and Fülöp, V., In *Crystallographic Computing 5: From Chemistry to Biology* (D. Moras, A.D. Podjarny and J.C. Thierry, Eds.), pp. 29-49, Oxford Science Publications, New York.

89. Calibration and correction of spatial distortions in 2D detector systems (1996), Hammersley, A. P., Svensson, S. O. and Thompson, A., *Nucl. Instrum. Meth.*, **A346**, 312-321.

90. Towards automatic indexing of the Laue diffraction pattern (1996), Ravelli, R. B. G., Hezemans, A. M. F., Krabbendam, H. and Kroon, J., *J. Appl. Cryst.*, **29**, 270-278.

91. Quantitative analysis of synchrotron Laue diffraction patterns in macromolecular crystallography (1995), Ren, Z. and Moffat, K., *J. Appl. Cryst.*, **28**, 461-481.

92. Deconvolution of energy overlap in Laue diffraction patterns in macromolecular crystallography (1995), Ren, Z. and Moffat, K., *J. Appl. Cryst.*, **28**, 482-493.

93. Crystallographic *R* Factor refinement by molecular dynamics (1987), Brünger, A. T., Kuriyan, J. and Karplus, M., *Science*, **235**, 458-460.

94. Application of maximum likelihood methods for macromolecular refinement (1996), Murshudov, G. N., Dodson, E. J. and Vagin, A. A., In *Macromolecular Refinement, Proceedings of the CCP4 Study Weekend January 1996* (E. Dodson, M. Moore, A. Ralph and S. Bailey, Eds.), pp. 93-104, CCLRC, Daresbury.

95. Improved methods for building protein models in electron density maps and the location of errors in these models (1991), Jones, T. A., Zou, J.-Y., Cowan, S. W. and Kjeldgaard, M., *Acta Cryst.*, **A47**, 110-119.

96. Accuracy of structural information obtained at the ESRF from very rapid Laue data collection on macromolecules (1997), Bourgeois, D., Longhi, S., Wulff, M. and Cambillau, C., *J. Appl. Cryst.*, **30**, 153-163.

97. Structure refinement against synchrotron Laue data: strategies for data collection and reduction (1997), Yang, X., Ren, Z. and Moffat, K., *Acta Cryst.*, **D54**, 367-377.

98. Structure of a protein photocycle intermediate by millisecond time-resolved crystallography (1997), Genick, U. K., Borgstahl, G. E. O., Ng, K., Ren, Z., Pradervand, C., Burke, P. M., Srajer, V., Tsu-Yi Teng, T.-Y., Schildkamp, W., McRee, D. E., Moffat, K. and Getzoff, E. D., *Science*, **275**, 1471-1475.

99. Calcium binding sites in tomato bushy stunt virus visualized by Laue crystallography (1990), Campbell, J. W., Clifton, I. J., Greenhough, T. J., Hajdu, J., Harrison, S. C., Liddington, R. C. and Shrive, A. K., *J. Mol. Biol.*, **214**, 627-632.

100. Direct determination of acetyl-enzyme intermediate in the acetylcholinesterase-catalyzed hydrolysis of acetylcholine and acetylthiocholine (1984), Froede, H. C. and Wilson, I. B., *J. Biol. Chem.*, **259**, 11010-11013.

101. Checking your imagination: applications of the free R value (1996), Kleywegt, G. J. and Brünger, A. T., *Structure*, **4**, 897-904.

102. The pharmacotherapy of Alzheimer's disease based on the cholinergic hypothesis: an update (1995), Weinstock, M., *Neurodegeneration*, **4**, 349-356.

103. Brain selective inhibition of acetylcholinesterase: a novel approach to therapy for Alzheimer's disease (1993), Enz, A., Amstutz, R., Boddeke, H., Gmelin, G. and Malanowski, J., *Prog. Brain Res.*, **98**, 431-438.

104. Molecular and cellular biology of cholinesterases (1993), Massoulié, J., Pezzementi, L., Bon, S., Krejci, E. and Vallette, F.-M., *Prog. Neurobiol.*, **14**, 31-91.

105. The effect of elimination of intersubunit disulfide bonds on the activity, assembly, and secretion of recombinant human acetylcholinesterase. Expression of acetylcholinesterase Cys-580----Ala mutant (1991), Velan, B., Grosfeld, H., Kronman, C., Leitner, M., Gozes, Y., Lazar, A., Flashner, Y., Marcus, D., Cohen, S. and Shafferman, A., *J. Biol. Chem.*, **266**, 23977-23984.

106. N-glycosylation of human acetylcholinesterase: effects on activity, stability and biosynthesis (1993), Velan, B., Kronman, C., Ordentlich, A., Flashner, Y., Leitner, M., Cohen, S. and Shafferman, A., *Biochem. J.*, **296**, 649-656.

107. Soluble monomeric acetylcholinesterase from mouse: expression, purification, and crystallization in complex with fasciculin (1996), Marchot, P., Ravelli, R. B. G., Raves, M. L., Bourne, Y., Vellom, D. C., Kanter, J., Camp, S., Sussman, J. L. and Taylor, P., *Protein Sci.*, **5**, 672-679.

108. Interactions underlying subunit association in cholinesterases (1997), Giles, K., *Protein Eng.*, **10**, 677-685.

109. Production and secretion of high levels of recombinant human acetylcholinesterase in cultured cell lines: microheterogeneity of the catalytic subunit (1992), Kronman, C., Velan, B., Gozes, Y., Leitner, M., Flashner, Y., Lazar, A., Marcus, D., Sery, T., Papier, Y., Grosfeld, H., Cohen, S. and Shafferman, A., *Gene*, **121**, 295-304.

110. Fasciculins, anticholinesterase toxins from the venom of the green mamba *Dendroaspis angusticeps* (1984), Karlsson, E., Mbugua, P. M. and Rodriguez-Itthurralde, D., *J. Physiol. (Paris)*, **79**, 232-240.

111. Structure of acetylcholinesterase complexed with the anti-Alzheimer drug E2020 (Aricept") (1999), Kryger, G., Silman, I. and Sussman, J. L., *Structure*, (in press).

112. Crystallographic refinement by simulated annealing. Application to a 2.8 Å resolution structure of aspartate aminotransferase (1988), Brünger, A. T., *J. Mol. Biol.*, **203**, 803-816.

113. Cross-validated maximum likelihood enhances crystallographic simulated annealing refinement (1997), Adams, P. D., Pannu, N. S., Read, R. J. and Brünger, A. T., *Proc. Natl. Acad. Sci. USA*, **94**, 5018-5023.

114. Engineering resistance to 'aging' of phosphylated human acetylcholinesterase: role of the hydrogen bond network in the active center (1993), Ordentlich, A., Kronman, C., Barak, D., Stein, D., Ariel, N., Marcus, D., Velan, B. and Shafferman, A., *FEBS Lett.*, **334**, 215-220.

115. Aging of phosphylated human acetylcholinesterase: catalytic processes mediated by aromatic and polar residues of the active center (1996), Shafferman, A., Ordentlich, A., Barak, D., Stein, D., Ariel, N. and Velan, B., *Biochem. J.*, **318**, 833-840.

116. Classical electrostatics in biology and chemistry (1995), Honig, B. H. and Nicholls, A., *Science*, **268**, 1144-1149.

117. Gliotactin, a novel transmembrane protein on peripheral glia, is required to form the blood-nerve barrier in *Drosophila* (1995), Auld, V. J., Fetter, R. D., Broadie, K. and Goodman, C. S., *Cell*, **81**, 757-767.

118. *Drosophila* neurotactin mediates heterophilic cell adhesion (1990), Barthalay, Y., Hipeau-Jacquotte, R., de la Escalera, S., Jimenez, F. and Piovant, M., *EMBO J.*, **9**, 3603-3609.

119. Neuroligin 1: a splice site-specific ligand for beta-neurexins (1995), Ichtchenko, K., Hata, Y., Nguyen, T., Ullrich, B., Missler, M., Moomaw, C. and Sudhof, T. C., *Cell*, **81**, 435-443.

120. Cholinesterase-like domains in enzymes and structural proteins: functional and evolutionary relationships and identification of a catalytically essential aspartic acid (1991), Krejci, E., Duval, N., Chatonnet, A., Vincens, P. and Massoulié, J., *Proc. Natl. Acad. Sci. USA*, **88**, 6647-6651.

121. External and internal electrostatic potentials of cholinesterase models (1997), Felder, C. E., Silman, I., Lifson, S., Botti, S. A. and Sussman, J. L., *J. Molec. Graphics & Modelling*, **15**, 318-327.

122. Acetylcholinesterase: effects of ionic strength and dimerization on the rate constants (1994), Antosiewicz, J., Gilson, M. K. and McCammon, J. A., *Israel J. Chem.*, **34**, 151-158.

123. Electrooptical measurements demonstrate a large permanent dipole moment associated with acetylcholinesterase (1996), Pörschke, D., Créminon, C., Cousin, X., Bon, C., Sussman, J. L. and Silman, I., *Biophys. J.*, **70**, 1603-1608.

124. Electrostatic attraction by surface charge does not contribute to the catalytic efficiency of acetylcholinesterase (1994), Shafferman, A., Ordentlich, A., Barak, D., Kronman, C., Ber, R., Bino, T., Ariel, N., Osman, R. and Velan, B., *EMBO J.*, **13**, 3448-3455.

125. Acetylcholinesterase: role of the enzyme's charge distribution on steering of charged ligands towards the bottom of the reactive site gorge (1996), Antosiewicz, J., Wlodek, S. T. and McCammon, J. A., *Biopolymers*, **39**, 85-94.

126. Electric potentials in trypsin isozymes (1989), Soman, K., Yang, A. S., Honig, B. and Fletterick, R., *Biochemistry*, **28**, 9918-9926.

127. The α/β hydrolase fold (1992), Ollis, D. L., Cheah, E., Cygler, M., Dijkstra, B., Frolow, F., Franken, S. M., Harel, M., Remington, S. J., Silman, I., Schrag, J., Sussman, J. L., Verschueren, K. H. G. and Goldman, A., *Protein Eng.*, **5**, 197-211.

128. Relationship between sequence conservation and three-dimensional structure in a large family of esterases, lipases, and related proteins (1993), Cygler, M., Schrag, J. D., Sussman, J. L., Harel, M., Silman, I., Gentry, M. K. and Doctor, B. P., *Protein Sci.*, **2**, 366-382.

129. *Drosophila* neurotactin, a surface glycoprotein with homology to serine esterases, is dynamically expressed during embryogenesis (1990), Hortsch, M., Patel, N. H., Bieber, A. J., Traquina, Z. R. and Goodman, C. S., *Development*, **110**, 1327-1340.

130. Protein modelling by e-Mail (1995), Peitsch, M. C., *Bio/Technology*, **13**, 658-660.

131. 1.8 A refined structure of the lipase from *Geotrichum candidum* (1993), Schrag, J. D. and Cygler, M., *J. Mol. Biol.*, **230**, 575-591.

132. Calculation of the electric potential in the active site cleft due to alpha-helix dipoles (1982), Warwicker, J. and Watson, H. C., *J. Mol. Biol.*, **157**, 671-679.

133. Calculation of the total electrostatic energy of a macromolecular system: solvation energies, binding energies, and conformational analysis (1988), Gilson, M. K. and Honig, B., *Proteins*, **4**, 7-18.

134. Protein folding and association: insights from the interfacial and thermodynamic properties of hydrocarbons (1991), Nicholls, A., Sharp, K. and Honig, B., *Proteins: Struct. Funct. Genetics*, **11**, 281-296.

135. Structure of uncomplexed and linoleate-bound *Candida cylindracea* cholesterol esterase (1995), Ghosh, D., Wawrzak, Z., Pletnev, V. Z., Li, N., Kaiser, R., Pangborn, W., Jornvall, H., Erman, M. and Duax, W. L., *Structure*, **3**, 279-88.

136. Molecular cloning and expression of cDNA for rat pancreatic cholesterol esterase (1989), Kissel, J. A., Fontaine, R. N., Turck, C. W., Brockman, H. L. and Hui, D. Y., *Biochim. Biophys. Acta*, **1006**, 227-236.

137. Detecting folding motifs and similarities in protein structures (1997), Kleywegt, G. J. and Jones, T. A., *Methods in Enzym.*, **277**, 525-545.

138. A 240-fold electrostatic rate-enhancement for acetylcholinesterase-substrate binding can be predicted by the potential within the active-site (1996), Zhou, H. X., Briggs, J. M. and McCammon, J. A., *J. Am. Chem. Soc.*, **118**, 13069-13070.

139. Cholinesterases in avian neurogenesis (1994), Layer, P. G. and Willbold, E., *Int. Rev. Cytol.*, **151**, 139-181.

140. Cholinesterases regulate neurite growth of chick nerve cells *in vitro* by means of a non-enzymatic mechanism (1993), Layer, P. G., Weikert, T. and Alber, R., *Cell Tissue Res.*, **273**, 219-226.

141. Allosteric modulation of acetylcholinesterase activity by peripheral ligands involves a conformational transition of the anionic subsite (1995), Barak, D., Ordentlich, A., Bromberg, A., Kronman, C., Marcus, D., Lazar, A., Ariel, N., Velan, B. and Shafferman, A., *Biochemistry*, **34**, 15444-15452.

142. Acetylcholinesterase promotes regeneration of neurites in cultured adult neurons of *Aplysia*. (1997), Srivatsan, M. and Peretz, B., *Neuroscience*, **77**, 921-931.

143. Acetylcholinesterase accelerates assembly of amyloid-beta-peptides into Alzheimer's fibrils: possible role of the peripheral site of the enzyme (1996), Inestrosa, N. C., Alvarez, A., Perez, C. A., Moreno, R. D., Vicente, M., Linker, C., Casanueva, O. I., Soto, C. and Garrido, J., *Neuron*, **16**, 881-891.

144. The structure-function relationships in *Drosophila* neurotactin show that cholinesterasic domains may have adhesive properties (1996), Darboux, I., Barthalay, Y., Piovant, M. and Hipeau-Jacquotte, R., *EMBO J.*, **15**, 4835-4843.

145. Electrostatic complementarity at protein/protein interfaces (1997), McCoy, A. J., Epa, V. C. and Colman, P. M., *J. Mol. Biol.*, **268**, 570-584.

146. Rapid, electrostatically assisted association of proteins (1996), Schreiber, G. and Fersht, A. R., *Nature Struct. Biol.*, **3**, 427-431.

147. Protein Data Bank (PDB): database of 3D structural information of biological macromolecules (1998), Sussman, J. L., Lin, D., Jiang, J., Manning, N. O., Prilusky, J., Ritter, O. and Abola, E. E., *Acta Cryst.*, **D54**, 1078-1084.

148. Reconsideration of the catalytic center and mechanism of mammalian paraoxonase/arylesterase (1995), Sorenson, R. C., Primo-Parmo, S. G., Kuo, C.-L., Adkins, S., Lockridge, O. and La Du, B. N., *Proc. Natl. Acad. Sci. USA*, **92**, 7187-7191.

149. Enzymes hydrolyzing organophosphates as potential catalytic scavengers against organophosphate poisoning (1998), Masson, P., Josse, D., Lockridge, O., Viguié, N., Taupin, C. and Buhler, C., *J. Physiol. (Paris)*, **92**, 357-362.

150. Production of human secretory component with dimeric IgA binding capacity using viral expression systems (1995), Rindisbacher, L., Cottet, S., Wittek, R., Kraehenbuhl, J.-P. and Corthésy, B., *J. Biol. Chem.*, **270**, 14220-14228.

151. Recombinant carbohydrate and selenomethionl variants of human choriogonadotropin (1991), Chen, W. and Bahl, O. P., *J. Biol. Chem.*, **266**, 8192-8197.

152. Determination of macromolecular structures from anomalous diffraction of synchrotron radiation (1991), Hendrickson, W. A., *Science*, **254**, 51-58.

153. Properties of the retained N-terminal hydrophobic leader sequence in human serum paraoxonase/arylesterase (1998), Sorenson, R. C., Aviram, M., Bisgaier, C. L., Billecke, S., Hsu, C. and La Du, B. N., *Abstracts of Third International Meeting on Esterases Reacting with Organophosphorus Compounds*, P21.

154. Purification and characterization of recombinant histidine-tagged human platelet 12-lipoxygenase expressed in a baculovirus/insect cell system (1993), Chen, X. S., Brash, A. R. and Funk, C. D., *Eur. J. Biochem.*, **214**, 845-852.

155. *Baculovirus expression vector system manual* (1998), Crossen, R. and Gruenwald, S., Pharmingen, San Diego.